Local actin nucleation tunes centrosomal microtubule nucleation during passage through mitosis

Francesca Farina*[1,3,5], Nitya Ramkumar*^[1], Louise Brown[2], Durren Samander-Eweis[1], Jannis Anstatt[1], Thomas Waring[2], Jessica Bithell[2], Giorgio Scita[3,6], Manuel Thery[4], Laurent Blanchoin[5], Tobias Zech[2], Buzz Baum^[1]

1. MRC-LMCB, UCL, London
2. Institute of Translational Medicine, Cellular and Molecular Physiology, University of Liverpool, Liverpool, England, UK
3. IFOM, the FIRC Institute of Molecular Oncology and University of Milan, Milan
4. Hospital Saint-Louis, Paris
5. University of Grenoble
6. Department of Oncology and Hemato-Oncology, University of Milan, Milan, Italy.

* These authors contributed equally
^ Please address all correspondence to these authors: b.baum@ucl.ac.uk, n.ramkumar@ucl.ac.uk

Cells going through mitosis undergo precisely timed changes in cell shape and organisation, which serve to ensure the fair partitioning of cellular components into the two daughter cells. These structural changes are driven by changes in actin filament and microtubule dynamics and organisation. While most evidence suggests that the two cytoskeletal systems are remodelled in parallel during mitosis, recent work in interphase cells has implicated the centrosome in both microtubule and actin nucleation, suggesting the potential for regulatory crosstalk between the two systems. Here, by using both *in vitro* and *in vivo* assays to study centrosomal actin nucleation as cells pass through mitosis, we show that mitotic exit is accompanied by a burst in cytoplasmic actin filament formation that depends on WASH and the Arp2/3 complex. This leads to the accumulation of actin around centrosomes as cells enter anaphase and to a corresponding reduction in the density of centrosomal microtubules. Taken together, these data suggest that the mitotic regulation of centrosomal WASH and the Arp2/3 complex controls local actin nucleation, which may function to tune the levels of centrosomal microtubules during passage through mitosis.

Running Title - Mitotic regulation of centrosomal actin

Keywords- Centrosomal actin, mitosis, Arp2/3 complex, WASH complex

Introduction

The microtubule (Zhai *et al*, 1996; Meraldi & Nigg, 2002) and actin cytoskeletons (Ramkumar & Baum, 2016) undergo profound parallel changes in dynamics and organisation as cells go through mitosis. These changes play a vital role in the control of animal cell division and begin as cells enter prophase. At this time, the interphase microtubule cytoskeleton is disassembled (Mchedlishvili *et al*, 2018; Niethammer *et al*, 2007; Centonze & Borisy, 1990), allowing microtubule nucleation to become focused at centrosomes (Zhai *et al*, 1996; Piehl *et al*, 2004; Mchedlishvili *et al*, 2018), where gamma-tubulin accumulates (Bettencourt-Dias & Glover, 2007; Khodjakov & Rieder, 1999; Sulimenko *et al*, 2017). With the loss of the nuclear/cytoplasmic compartment barrier at the onset of prometaphase, this is followed by a sudden change in microtubule organization (Mchedlishvili *et al*, 2018) and dynamics (Zhai *et al*, 1996). During prometaphase, the short, dynamic centrosomal microtubules that remain capture chromosomes (Mitchison & Kirschner, 1985), drive bipolar spindle formation (Magidson *et al*, 2011) and interact with the cortex to guide positioning of the mitotic spindle (McNally, 2013).

The actin cytoskeleton also undergoes changes over the same period. These begin in prophase when the interphase actin cytoskeleton is disassembled (Matthews *et al*, 2012). This likely frees up a pool of actin monomers (Kaur *et al*, 2014), which is then used to assemble the thin (Clark *et al*, 2013), mechanically rigid (Fischer-Friedrich *et al*, 2015), cortical actomyosin network that drives mitotic rounding (Reinsch & Karsenti, 1994; Sorce *et al*, 2015; Ragkousi & Gibson, 2014). While the mechanisms underlying this mitotic switch in actin organisation are not well understood, the process likely involves: i) the loss of interphase focal adhesions (Dix *et al*, 2018; Lock *et al*, 2018), ii) the loss of Arp2/3-dependent lamellipodia (Ibarra *et al*, 2005; Bovellan *et al*, 2014; Rosa *et al*, 2015), and iii) the activation of formins downstream of Ect2/Pbl and the GTPase Rho (Matthews *et al*, 2012; Maddox & Burridge, 2003; Rosa *et al*, 2015; Chugh *et al*, 2017).

Interestingly, these parallel changes in actin and microtubule organisation appear to be largely independent of one another (Mchedlishvili *et al*, 2018). Thus, mitotic rounding is not much altered in cells entering mitosis without microtubules. Conversely, mitotic spindle assembly occurs with relatively normal kinetics in spherical cells that have been treated with latrunculin to remove their actomyosin cortex (Lancaster et al, 2013). Thus, during mitotic entry, the two systems appear to be independently regulated. However, this changes at anaphase, where the behaviour of the two filament systems is tightly coordinated for proper cell division. The signals emanating from the anaphase spindle polarises the overlying actomyosin cortex (Rappaport, 1996). This is achieved mainly through the activity of the centralspindlin complex (White & Glotzer, 2012), which binds overlapping microtubules at the midzone. This complex, in turn, recruits Ect2 (Su et al, 2011; Yüce et al, 2005), leading to Rho activation and assembly of a contractile actomyosin ring (Rappaport, 1996; Fededa & Gerlich, 2012), which drives cytokinesis (Wagner & Glotzer, 2016; Basant & Glotzer, 2018). At the same time, as the anaphase spindle elongates, signals associated with the anaphase chromatin appear to aid relaxation of the polar cortical actomyosin network (Ramkumar & Baum, 2016). This leads to the de-phosporylation of ERM proteins, which crosslink

actin to the plasma membrane (Motegi *et al*, 2006; Salmon & Wolniak, 1990; Rodrigues *et al*, 2015; von Dassow, 2009), to the loss of Anillin (Kiyomitsu & Cheeseman, 2013), and to activation of SCAR/WAVE and the Arp2/3 complex at opposing cell poles (Bastos et al, 2012; Nezis et al, 2010; Luo et al, 2014; King et al, 2010; Zhang & Robinson, 2005). In some instances, the process of polar relaxation and cell re-spreading are sufficient to drive division in cells that lack an actomyosin ring (Dix et al, 2018; King et al, 2010; Neujahr et al, 1997).

In studies looking at the role of the actin cytokskeleton in division, the mitotic cortical actomyosin network has been subject to most scrutiny. This is because cortical cytoskeleton controls animal cell shape and is by far the brightest actin-based structure visible under the microscope. However, two groups have reported the existence of dynamic cytoplasmic actin-based structures in dividing HeLa cells (Mitsushima *et al*, 2010; Field & Lénárt, 2011; Fink *et al*, 2011). While the precise function of this pool of cytoplasmic actin remains unclear, it has been reported to play a role in spindle assembly and positioning in various systems (Woolner *et al*, 2008; Sabino *et al*, 2015). In addition, at anaphase, this pool of cytoplasmic actin appears to work together with an unconventional Myosin, Myo19, to aid the precise and fair partitioning of mitochondria at anaphase (Rohn *et al*, 2014).

Here, building on a previous study that identified the WASH/Arp2/3-dependent nucleation of actin at centrosomes in interphase cells (Farina *et al*, 2016), we have re-examined the dynamics and potential function of non-cortical actin at mitotic exit. Using a combination of cell biology and biochemistry, we report the identification of a pool of WASH/Arp2/3-dependent cytoplasmic actin that is nucleated around centrosomes in early anaphase, which appears to limit the nucleation of centrosomal microtubules.

Results

In order to explore the possibility that actin is nucleated at centrosomes during mitotic exit, as it is in interphase cells (Farina *et al*, 2016), we fixed a population of HeLa cells and examined the amount of F-actin (Phalloidin) and microtubules in a region close to centrosomes at different cell cycle stages. This revealed an increase in the density of F-actin in a small region around the centrosomes during the passage from metaphase to early anaphase (Figure 1A-B). During this period, we observed no significant changes in the levels of non-centrosomal cytoplasmic actin (Figure EV1A,C). This increase in centrosomally-associated actin was accompanied by a decrease in microtubules intensity in the same region (Figure 1A, EV1B). A similar increase in actin accumulation and a corresponding decrease in tubulin intensity were also observed around the centrosomes of early anaphase Jurkat cells, a T-lymphocyte cell line (Figure EV1E-F). To investigate the dynamics of actin during this period, we used a spinning disk confocal to image HeLa cells expressing Lifeact-GFP. We observed a dynamic pool of cytoplasmic actin in metaphase, as described previously (Fink *et al*, 2011; Mitsushima *et al*, 2010). At anaphase, this pool became concentrated sub-cortically around the opposing poles (Figure 1C, Figure EV2, Movies EV1-3). In order to define the dynamics of actin accumulation around the centrosomes, we generated a stable Hela cell line expressing RFP-LifeAct and GFP-Tubulin and performed relatively high temporal resolution acquisition (Figure 1D). Shortly after anaphase onset, we observed an increase in the levels of actin around centrosomes (Figure 1D-F), while non-centrosomal cytoplasmic actin levels remained unchanged (Figure EV 1A,D). This burst of actin filament formation was extremely transient, occurring within minutes of anaphase onset, and was over by the time the cytokinetic furrow became clearly visible (Figure 1C-F, Figure EV2, Movies EV1-3). Further, we observed this transient accumulation of actin around centrosomes during anaphase using diverse actin reporters (siR-actin, Lifeact-GFP and RFP-Lifeact), albeit with different accumulation dynamics that we attribute to the nature of the probes and their differing actin binding kinetics (Figure 1, Figure EV2). During the same period, the density of microtubules, measured as an integrated intensity in a small region around spindle poles, dropped (Figure 1D, G). Thus, this transient appearance of cytoplasmic actin close to centrosomes at mitotic exit is associated with a reduction in the density of centrosomal microtubules.

In order to better visualize centrosomal actin *in vivo,* and as a method by which to isolate centrosomes for the *in vitro* experiments (see below), we also carried out similar analysis during monopolar cytokinesis (Hu *et al*, 2008). For these experiments, we arrested HeLa cells in prometaphase using STLC (DeBonis *et al*, 2004; Mayer *et al*, 1999) – a treatment that inhibits the Eg5 motor to prevent the assembly of a bipolar spindle (Figure 2). Actin nucleation was then followed as these prometaphase-arrested cells were forced to exit mitosis through the addition of a Cdk1 inhibitor (RO-3306) (Hu *et al*, 2008). Importantly, under these conditions, the analysis of centrosomal actin is facilitated by the fact that the monopole contains both centrosomes and remains far from the cell cortex (Figure 2A) – even though many other aspects of cytokinesis appear similar (Karayel *et al*, 2018).. In this experiment, we observed little centrosomal-associated actin in the cells arrested in prometaphase with STLC (Figure 2A, Figure EV3, Movie EV4). However, within ~6 minutes of Cdk1 inhibitor addition we observed a burst of actin filament formation

close to centrosomes (Figure 2A, Figure EV3, Movie EV4). Strikingly, these actin filaments formed parallel bundles that lay in between the astral microtubules emanating from the large monopole present in these cells (Figure 2A-B). To confirm this finding, cells arrested in prometaphase and cells post forced exit were fixed and stained to visualise actin filaments (Phalloidin). Similar to the live cells here also we observed an increase in actin around centrosomes during forced exit in multiple cell lines: in HeLa cells (Figure 2C-E), the Jurkat T-cell line (Figure EV4A-B) and in the MAVER1 B-cell line (Figure EV4C-D). Further, this actin accumulation was accompanied by a reduction in the density of centrosomal microtubules (Figure 2E). Thus, cytoplasmic actin appears to transiently accumulate around centrosomes during mitotic exit during both monopolar and bipolar divisions and this is accompanied by a local decrease in microtubule density.

Previous work demonstrated that the actin formed at interphase centrosomes is nucleated by a local pool of Arp2/3 (Farina et al., 2016). To investigate the role of Arp2/3 complex in actin accumulation during mitotic exit, we treated cells with either DMSO or the Arp2/3 complex inhibitor, CK666 and determined the amount of centrosomal actin in fixed (Figure 3) and live cells (Figure EV5). While the DMSO control behaved as described above, the CK666 Arp2/3 inhibitor was effective in eliminating the formation of cytoplasmic actin, including the actin emanating from the centrosome (Figure 3A-D). This was the case in both regular bipolar mitosis (Figure 3A-B), forced monopolar exit (Figure 3C-D) and live monopolar exit (Figure EV5A-B). Interestingly, while the actin accumulation was decreased with the Arp2/3 inhibitor, we found that Arp2/3 inhibition also prevented the reduction in the density of microtubules associated with centrosomes during normal mitotic exit (Figure 3E, EV6A) and in a monopolar exit (fixed cells-Figure 3F,6B; live cells- EV5C). This suggests that the pool of actin associated with the centrosomes may influence the centrosomal microtubule in early anaphase. This could be essential to ensure proper cytokinesis, as we observed a small percentage of cells with spindle oscillations.

These results indicate a role for Arp2/3 in generating the burst of cytoplasmic actin associated with centrosomes at mitotic exit. To determine the localization dynamics of Arp2/3 during mitotic progression, we fixed and stained cells using an antibody against a component of the complex, p34 (Figure 4A). This revealed a pool of Arp2/3 at the centrosome, marked by Centrin 1 (Figure 4A) that was very low to undetectable in metaphase, but increased significantly in intensity as cells were forced to leave mitosis (Figure 4B). A similar increase in the level of centrosomal Arp2/3 was also observed when we analysed the association of p34 with centrosomes purified from cells before and shortly after forced mitotic exit (Figure 4C-D). Additionally, we observed a pool of Arp2 colocalised with Centrin at the centre of centrosomes, which was significantly higher during anaphase (Figure EV7A-B'). These data identify a pool of Arp2/3 that is recruited to centrosomes soon after the onset of anaphase, where it functions to nucleate the formation of local actin filaments.

To validate these findings and to determine whether centrosomes might be a potential source of the cytoplasmic pool of actin formed at anaphase, we performed biochemical experiments on centrosomes isolated from cells arrested in prometaphase and those treated with the Cdk1 inhibitor (see methods and Farina *et al*, 2016). While centrosomes isolated from prometaphase cells failed to nucleate

significant levels of actin, centrosomes isolated from cells shortly after forced exit from mitosis nucleated large actin asters (Figure 4E-F). Significantly, the *in vitro* growth of these actin asters could be inhibited by the addition of Capping protein (Figure 4G-H), which caps the growing plus ends of filaments (Pollard & Borisy, 2003), as expected if they were formed as the result of active Arp2/3 localised at the centrosome. Further, when we washed-out Capping protein and switched the colour of the labelled monomeric actin in the solution, we were able to show that this actin was nucleated at the centre of the aster at the centrosome (yellow dot in Figure 4G). Finally, we used CK666 to confirm that the formation of these actin asters was dependent on Arp2/3 complex activity (Figure 4I-J), as it was in cells exiting mitosis.

Next we turned to WASH to determine whether this anaphase pool of centrosomal actin filament formation depends on the WASH complex, as was previously described for interphase cells (Farina *et al*, 2016). To begin, we used Western blotting to follow WASH1 in interphase cells, mitotic cells or cells following forced mitotic exit (Figure 5A-B). This revealed a clear CDK1-dependant band-shift, in line with the idea that WASH is modified by phosphorylation (Olsen *et al*, 2010). In addition, we were able to see a shift in the size of the WASH1 complex on a native gel, during monopolar cytokinesis, suggesting the possibility that there are larger changes in the WASH complex at the transition between metaphase and anaphase (Figure 5B). Finally, we observed a slight elevation of WASH1 signal around centrosomes when we imaged WASH1 localization in prometaphase arrested cells and in cells forced to exit mitosis (Figure EV7C).

To test whether WASH complex also plays a function in generating the burst of centrosomal actin filament formation at anaphase, we performed WASH1 RNAi (confirmed by Western blot (Figure 6C)). For this experiment, WASH1 RNAi cells were arrested in STLC and then released (Figure 6A-B) to avoid the impact of WASH RNAi on mitotic entry. When the levels of centrosomal actin were then compared in control and WASH RNAi cells as they exited mitosis, we observed a near complete loss of centrosomal actin in cells exiting mitosis, both in live (Figure 6A-B) and in fixed samples (Figure 6D-E). Moreover, we observed a similar loss in the ability of centrosomes to nucleate actin asters when we pre-treated purified centrosomes with anti-WASH1 antibody (Figure 6F-G). Thus, both *in vivo* and *in vitro*, WASH RNAi appears to have the same effect as a treatment with the Arp2/3 inhibitor, CK666.

Discussion

This paper identifies a role for Arp2/3 and its upstream activator, WASH complex, in the nucleation of actin filaments from centrosomes at mitotic exit. While it has long been clear that the spindle directs the assembly of a contractile actomyosin ring at anaphase, and that actin and microtubules work together to control cell shape and organization (Huber *et al*, 2015), there has been little evidence of crosstalk between the two filament systems occurring in the opposite direction during mitosis. The data presented here, along with data in studies carried out in lymphocytes in interphase (Inoue *et al*, 2019) and in *Xenopus* egg extracts *in vitro* (Colin *et al*, 2018), suggest that actin may also play a role in tuning microtubule nucleation at the centrosome.

There are many ways in which the microtubule network can be influenced by actin filaments (Rodriguez *et al*, 2003; Coles & Bradke, 2015; Huber *et al*, 2015; Colin *et al*, 2018). Actin can direct the growth and alignment of microtubules (Thery *et al*, 2006; López *et al*, 2014; Kaverina *et al*, 1998; Elie *et al*, 2015), can change MT dynamics (Zhou *et al*, 2002; Hutchins & Wray, 2014), and can subject MTs to mechanical forces and physical constraints (Gupton *et al*, 2002; Fakhri *et al*, 2014; Huber *et al*, 2015; Katrukha *et al*, 2017; Brangwynne *et al*, 2006; Robison *et al*, 2016; Colin *et al*, 2018). These interactions occur along the length of microtubules and at their growing plus ends (Mohan & John, 2015; Akhmanova & Steinmetz, 2015), and are especially prevalent at the cell periphery (Waterman-Storer & Salmon, 1997; Wittmann *et al*, 2003), where the two filament systems converge in a crowded space.

The presence of actin at the centrosome (Farina *et al*, 2016) now provides an additional spatial region where the two filaments systems can interact to regulate one another's behaviour. Here we show that centrosomal actin is generated through the local recruitment and utilization of the Arp2/3 complex during anaphase. This is likely to be regulated by the change in Cdk1 activity at mitotic exit. The anaphase burst of centrosomal actin is also dependent on the activity of the WASH complex. The timing of centrosomal actin nucleation correlates with the mitosis-specific WASH1 band-shift (Figure 5A-B), suggesting that this process might be regulated by mitotic kinases and phosphatases acting on WASH1. This could be augmented by the mitotic regulation of Arp2/3 complex. The precise nature of the activation of these complexes and their crosstalk remains to be determined.

Like Arp2/3 on a bead, bacterium or patch (Pollard & Borisy, 2003; Pollard *et al*, 2000; Reymann *et al*, 2011) the local activation of Arp2/3 is expected to generate actin filaments that have their minus ends fixed in place, while their plus-ends grow out into the cytoplasm (Figures 1-4, EV1-3). This is in keeping with the fact that the extension of these asters can be capped by Capping protein (Figure 4G). However, in cells exiting mitosis normally (Figure 1C-D, Figure EV2, Movies EV1-3), centrosomes also appear to nucleate a much more diffuse cytoplasmic pool of actin. This may result from Arp2/3-dependent branching of centrosomally-nucleated filaments in the cytoplasm of anaphase cells. Together, this pool of cytoplasmic WASH-Arp2/3 dependent actin may have an impact on the viscosity of the cytoplasm (Moulding *et al*, 2012), as has been shown in meiotic cells (Chaigne *et al*, 2016). This increased viscosity might act to limit the movement of separated organelles after the disassembly of the anaphase spindle – as has been shown for mitochondria (Rohn *et al*, 2014).

Previous studies have suggested mitotic roles for cytoplasmic actin in centrosome separation (Rosenblatt *et al*, 2004; Cao *et al*, 2010), pole splitting (Sabino *et al*, 2015), and spindle assembly (Woolner *et al*, 2008; Vilmos *et al*, 2016; Po'uha & Kavallaris, 2015). Our data suggests that the capacity for the generation of centrosomal actin in metaphase is limited. Moreover, in HeLa cells, where this cytoplasmic actin was first observed (Fink *et al*, 2011; Mitsushima *et al*, 2010), Arp2/3 complex activity doesn't influence the timing of mitotic progression (Lancaster *et al*, 2013) and contributes little to metaphase cortical mechanics (Chugh *et al*, 2017). However, our data support the idea that cytoplasmic actin has a significant function at the onset of anaphase (including in the control of mitochondrial

movement, (Rohn et al., 2014)), when CDK1-mediated phosphorylation of WASH is relieved and active Arp2/3 returns to the centrosome to induce a burst of actin.

This burst in centrosomal actin is accompanied by a reduction in the microtubule density around the centrosomes at early anaphase. In the absence of centrosomal actin nucleation, with Arp2/3 inhibitor, this reduction in microtubule density is inhibited. This suggests an antagonistic cross talk between the two filament systems at mitotic exit. The precise nature of this antagonism between local actin and microtubule formation at the centrosome remains to be determined (Obino *et al*, 2016; Piel *et al*, 2001; Inoue *et al*, 2019) . We speculate that this burst of anaphase actin nucleation at centrosomes may cause steric problems, as the two systems compete for physical space around the centrosome. However, in live cells, we cannot rule out the possibility of an indirect cross-talk mediated by either changes in localization and/or activity of proteins affecting post-translational modifications of tubulin during mitotic exit (Shi *et al*, 2019). Further, it is possible that the centrosomal actin pool could have a more profound effect depending on the nature of microtubules i.e. astral vs spindle microtubules at mitotic exit.

The reduction in microtubule density around centrosomes may help cells leaving mitosis to re-establish a telophase array of sparse, long centrosomal microtubules. These microtubules can then span the entire space of the cells, assisting in polar relaxation, adjusting spindle orientation (Kiyomitsu & Cheeseman, 2013), and/or promoting re-spreading (Ferreira *et al*, 2013). In short, this reduction in microtubule density at early anaphase could assist cells exiting mitosis to return to their interphase organization and morphology.

Acknowledgements:

NR, FF and BB thank CRUK. NR and BB thank BBSRC. LB (Louise) was funded by a Breast Cancer Now grant (2014MayPR292) to TZ. TW is funded by the NLD BBSRC doctoral training program (BB/M011186/1/1797330). TZ thanks the Institute of Translational Medicine Biomedical Imaging Facility. LB (Laurent) is supported by (ERC AAA 741773). GS thanks AIRC (IG#18621) and Italian Ministry of Health (RF-2013-02358446).

Author contributions:

NR carried out the cell culture experiments for normal bipolar cytokinesis in different cell lines, live imaging bipolar and monopolar cytokinesis. FF carried out the *in vitro* work and cell biological experiments shown in Figures (2, 3C, 4, 6, Supp 5). DS and JA helped with monopolar and bipolar cytokinesis experiments respectively. FF and BB conceived the initial idea. NR and BB oversaw the development of the project and wrote the manuscript with assistance from TZ. LB (Louise) and TZ did WASH biochemistry. TW, JB and TZ did the monopolar cytokinesis in Jurkat and MAVER1 cell lines. MT and LB (Laurent) oversaw in vitro work and advised on in vivo work, together with help from GS.

Conflict of interest:

The authors declare no conflict of interest.

Methods

Cell culture

HeLa Kyoto cells were cultured in DMEM, and Jurkat cells (immortalized human T lymphocytes) as well as MAVER1 CML B cells in RPMI 1640 (Gibco) at 37°C and 5% CO_2. All media were supplemented with 10% foetal bovine serum and penicillin/streptomycin (Gibco). Cells were synchronized in prometaphase using S-trityl-L-cysteine (STLC; Sigma) at 5μM treatment for 18 hr (Skoufias *et al*, 2006). Forced mitotic exit was performed by the addition of 20 μM Ro-3306 (Enzo Life Sciences), an inhibitor of Cdk1/cyclin B1 and Cdk1/cyclin A to STLC treated cells. For the Arp2/3 complex inhibition experiments, we used 0.2 mM CK666 (Sigma Aldrich). Control experiments were performed using DMSO. For CK666 treatment (Fig3), cells were plated with 2mM Thymidine for 22 hours, were released from Thymidine block for 9 hours, following which they were treated with DMSO or 0.2mM CK666 for 15 mins. They were then processed for staining. Actin network disruption was performed by adding 10 μg/ml cytochalasin D (Sigma Aldrich). Microtubules depolymerisation was performed by adding 1 μM nocodazole (Sigma Aldrich) for 1 hour at 37°C and 5% CO_2 and for 30 minutes at 4°C.

Stable and transient cell transfection

Stable HeLa cell lines expressing GFP-α-tubulin and RFP-Lifeact were established starting from HeLa stably expressing GFP-α-tubulin by lentiviral transduction with rLV-Lifeact-RFP (Ibidi) using 3 MOI (multiplicity of infection). After 24 hours cells were incubated with fresh medium for 48 hours. After 72 hours post-transduction, stable cells were selected using 1 μg/ml puromycin. Medium with puromycin was replaced every 2-3 days until resistant colonies were identified. ON-TARGETplus Human SMARTpool WASH1-targeting (siWASH1) siRNAs (Dharmacon, GE Healthcare) were transfected into HeLa cells at a final concentration of 20 nM using Lipofectamine RNAiMax (Life Technologies) according to supplier's protocol. Negative control siRNA was performed using AllStars Negative Control siRNA (Qiagen).

Isolation of centrosomes

Centrosomes were isolated from cells arrested in prometaphase (STLC) or shortly after their forced mitotic exit (Ro-3306 5') using a previously published protocol (Farina *et al*, 2016). Cells were incubated for 18 hours with STLC then treated with nocodazole (0.2 μM) and cytochalasin D (1 μg/ml). For the mitotic exit we added to STLC-treated cells 20 μM Ro-3306 for 5 minutes, and cells were kept on ice for 30 minutes. Centrosomes were then harvested by centrifugation onto a 60% sucrose cushion and further purified by centrifugation through a discontinuous (70%, 50% and 40%) sucrose gradient. Composition of sucrose solutions was based on TicTac buffer (10 mM Hepes, 16 mM Pipes (pH 6.8), 50 mM KCl, 5 mM $MgCl_2$, 1 mM EGTA). The TicTac buffer was supplemented with 0.1% Triton X-100 and 0.1% β-mercaptoethanol.

Protein expression and purification

Tubulin was purified from fresh bovine brain by three cycles of temperature-dependent assembly/disassembly in Brinkley Buffer 80 (BRB80 buffer: 80 mM Pipes pH 6.8, 1 mM EGTA and 1 mM $MgCl_2$) according to Shelanski (Shelanski, 1973). Fluorescent tubulin (ATTO-565-labeled tubulin) was prepared according to Hyman et al. (Hyman *et al*, 1991). Actin was purified from rabbit skeletal-muscle acetone powder (Spudich & Watt, 1971). Monomeric Ca-ATP-actin was purified by gel-filtration chromatography on Sephacryl S-300 (MacLean-Fletcher & Pollard, 1980) at 4 °C in G buffer (2 mM Tris-HCl, pH 8.0, 0.2 mM ATP, 0.1 mM $CaCl_2$, 1 mM NaN_3 and 0.5 mM dithiothreitol (DTT)). Actin was labelled on lysines with Alexa-488, Alexa-568 and Alexa-647 as described previously (Isambert *et al*, 1995; Egile *et al*, 1999). Recombinant human profilin, mouse capping protein, the Arp2/3 complex, GST-pWA and mDia1 were purified according to previous work (Almo *et al*, 1994; Falck *et al*, 2004; Machesky *et al*, 1999; Michelot *et al*, 2007; Egile *et al*, 1999).

In-vitro assay

This was done essentially as in Farina et al 2016. Briefly, experiments were performed in polydimethylsiloxane (PDMS) open chambers in order to sequentially add experimental solutions when needed. PDMS (Sylgard 184 kit, Dow Corning) was mixed with the curing agent (10:1 ratio), degased, poured into a Petri dish to a thickness of 5 mm and cured for 30 minutes at 100°C on a hot plate. PDMS layer was cut to 15 mm x 15 mm and punched using a hole puncher (ted Pella) with an outer diameter of 8 mm. The PDMS chamber and clean coverslip (20 mm x 20 mm) were oxidized in an oxygen plasma cleaner for 20 s at 80 W (Femto, Diener Electronic) and brought into contact. Isolated centrosomes were diluted in TicTac buffer (10 mM Hepes, 16 mM Pipes (pH 6.8), 50 mM KCl, 5 mM $MgCl_2$, 1 mM EGTA) and incubated for 20 minutes. Excess centrosomes were removed by rinsing the open chamber with large volume of TicTac buffer supplemented with 1% BSA to prevent the non-specific interactions (TicTac-BSA buffer). Microtubules and actin assembly at the centrosome was induced by diluting tubulin dimers (labelled with ATTO-565, 30 µM final) and/or actin monomers (labelled with Alexa-488, or Alexa-568, or Alexa-647, 1 µM final) in TicTac buffer supplemented with 1 mM GTP and 2.7 mM ATP, 10 mM DTT, 20 µg/ml catalase, 3 mg/ml glucose, 100 µg/ml glucose oxidase and 0.25 % w/v methylcellulose. In addition, a 3-fold molar equivalent of profilin to actin was added in the reaction mixture. Antibody inhibition experiments were performed by incubating isolated centrosomes with primary antibodies (diluted in TicTac-BSA buffer) for 1 hour. The control experiment without antibodies was performed incubating isolated centrosomes for 1 hour with TicTac-BSA buffer. Arp2/3 complex inhibition experiments were performed by adding 0.2 mM CK666 in the reaction mixture.

Immunofluorescence staining (in-cell)

This was done essentially as in Farina et al 2016. Briefly, cells were incubated for 18 hours with STLC. Forced mitotic exit was performed incubating STLC cells with Ro3306 for 5 minutes. Cells were then fixed and stained. For actin filament staining, cells were fixed with 4 % paraformaldehyde (PFA) for 20 minutes, blocked with antibody blocking buffer (PBS supplemented with 1 % BSA, PBS-BSA) for 30 minutes. Permeabilization was performed with 0.2 % Triton X-100 for 1 minute. Alexa-647-phalloidin (200 nM) was incubated for 20 minutes. DNA was labeled with

a 0.2 µg/ml solution of 4',6-diamidino-2-phenylindole dihydrochloride (DAPI) (Sigma). The coverslips were air-dried and mounted onto glass slides using Mowiol mounting medium. Arp2/3 staining was performed by fixing cells with methanol at -20°C for 3 minutes and blocking with PBS-BSA for 30 minutes. Primary and secondary antibodies, diluted in PBS-BSA, were incubated for 1 hour and 30 minutes respectively. DNA labeling and coverslip mounting were performed as previously described.

Immunofluorescence staining (isolated centrosomes)

This was done essentially as in Farina et al 2016. Briefly, staining of F-actin on centrosomes was performed without prior fixation. Isolated centrosomes were incubated with primary antibodies for 1 hour and with secondary antibodies for 30 minutes at room temperature. The antibodies were diluted in TicTac-BSA buffer.

Imaging, processing and analysis

This was done essentially as in Farina et al 2016. Briefly, fixed cell images were captured on a confocal microscope (Leica SP5) using a 40x 1.25 N.A. objective lens, 63X 1.4 N.A. or Zeiss LSM800 with a 63x 1.4 N.A. lens. Live cell imaging was performed on a UltraView Vox (Perkin Elmer) spinning disc confocal microscope with 60X NA 1.4 oil objective and 100X 1.4 N.A. and 3I spinning disc confocal with 63X 1.4 N.A and 100X 1.4 N.A objectives equipped with a temperature-controlled environment chamber. Image processing was performed using ImageJ software. All the images show the centrosome plane. Measurement of the actin amount around the centrosome was performed by measuring the integrated intensity of fluorescence in a 4 µm diameter circle centered around the centrosome. p34-Arc measurements were performed measuring the integrated fluorescence intensity in a 3 µm diameter circle centered around the centrosome. Data from separate experiments were normalized so that the average intensity in control cells was 1. Imaging of isolated centrosomes was performed with a Total Internal Reflection Fluorescence (TIRF) microscope (Roper Scientific) equipped by an iLasPulsed system and an Evolve camera (EMCCD 512 x 512, pixel = 16 µm) using a 60x 1.49 N.A objective lens. Actin nucleation activity was quantified measuring the actin fluorescence intensity integrated over a 2 µm diameter at the center of the actin aster and normalized with respect to initial intensity over the time. Representative data for several experiments are shown.

Actin staining and measurement bipolar divisions (Fig 1, 3):

Fixed cells- Cells were cultured in 96 well Cell carrier plates. For staining, cells were fixed with 4 % paraformaldehyde (PFA) for 20 minutes and permeabilized with 0.1 % Triton X-100 for 10 minutes. They were blocked in antibody blocking buffer (PBS supplemented with 5 % BSA, PBS-BSA) for 30 minutes and incubated with primary antibodies anti-tubulin (1:400) and anti-Pericentrin (1:1000) overnight at 4C. Cells were incubated with secondary antibodies – Goat anti-mouse-Alexa-647, goat anti-rabbit Alexa-568, Phalloidin FITC (1:500) and DAPI (4',6-diamidino-2-phenylindole dihydrochloride-1:1000) for 1 hour at room temperature. Jurkat cells were fixed with 4 % paraformaldehyde (PFA) for 20 minutes in suspension and were adhered to 96 well plates coated with Poly-L-lysine.

For analysis - A 4 µm diameter (for HeLa) and 3 µm diameter (for Jurkat) circle was centered around the centrosome using the pericentrin channel and the corresponding actin and tubulin integrated density around the same region was measured using Fiji. The images used were 2 *z*-projection around the centrosome plane. In order to combine data from multiple experiments, the data was normalized to metaphase average for each cell line. For live cells, a 4 µm diameter circle was centered around centrosomal region using alpha-tubulin RFP as reference. A 4 *z*-projection around centrosome region was used for measurements. The intensity data for each cell was normalized to the intensity at t=0, which is one frame before anaphase onset.

Actin measurement forced exit (Fig 2E-F, Fig EV1):

A circular, 3µm^2 ROI was centred on the centrosomes as determined by pericentrin staining. A series of slices equal to approximately 3µm in height (with z interval of 0.39µm the number of slices was 9, including the central slice) were then analysed using the defined ROI to give a mean intensity per slice, which were then averaged to give the mean intensity within the 3x3x3 cylindrical area. Individual cell averages were normalised to the experimental average for the STLC condition.

Statistics

Statistical analysis was performed with GraphPad Prism 7 (GraphPad Software). All graphs show mean and error bars are standard deviation. The test used is mentioned for each graph in figure legend. In all the graphs Prism convention: ns ($P > 0.05$), * ($P \leq 0.05$), ** ($P \leq 0.01$), *** ($P \leq 0.001$) and **** ($P \leq 0.0001$).

Western blotting

Western blots were performed fractioning proteins on SDS polyacrylamide gels. Membrane blocking was carried out using 3% BSA in PBS. Primary and secondary antibodies were diluted in PBS supplemented with 1% BSA and 0.1 % Tween-20 while washing steps were performed with PBS supplemented with 1% BSA and 1% Tween-20.

Blue NativePAGE

This was done essentially as in Tyrrell et al 2016 (Tyrrell *et al*, 2016). Briefly, cells were lysed using the NativePAGE™ Sample Prep Kit (Thermo Scientific – BN2008) Each sample was lysed in 400 µl of NP-lysis buffer [100 µl of NP-buffer, 260 µl of ddH_2O, 40 µl 5% digitonin, Halt protease inhibitor (Pearce) and halt phosphatase inhibitor(Pearce)] for 10 min on ice and scraped with a cell scraper. Samples were centrifuged at 20 000*g* for 30 min at 4°C, and pellets were discarded. Equal amounts of protein (determined using DC™ Protein Assay Kit (Bio-Rad-5000111)) were separated by BN-PAGE NativePAGE™ Novex™ 3–12% Bis-Tris Protein Gels as per the manufacturer's instructions ('NativePAGE™ Bis-Tris Gel protocol' from Thermo Scientific). NativeMark™ Unstained Protein Standard (ThermoFisher Scientific) was used as molecular weight standard. Protein was blotted onto PVDF membranes and fixed for 15 min in 8% acetic acid. Membranes were blocked in 5% milk for 1 h at room temperature and incubated overnight rocking at 4°C in 5% milk PBS-T. Membranes were washed in PBS-T and incubated for 1 h with

peroxidase-conjugated secondary antibody (Cell Signalling, Hitchin, UK). Clarity western blotting ECL substrate (BioRad) was used to generate a signal that was detected using a Chemidoc imaging system (BioRad).

Phos-tag band shifts

Cells were lysed using hot lysis buffer (2% SDS, 1mM EDTA, 50mMHaF, preheated to 97°C). Samples were allowed to cool at RT before performing protein assay using DC™ Protein Assay Kit (Bio-Rad-5000111). Sample buffer was added and equal protein was loaded into 8% polyacrylamide gels supplemented with 5µM Phos-tag and 10µM $MnCl_2$. Phos-tag gels were resolved at 30mA under constant current until the dye front migrated to the bottom of the gel. Gels were transferred onto nitrocellulose membrane with a 0.45 pore size (GE healthcare) at 250 mA for 120 mins under constant current.

Antibodies and chemicals

For immunofluorescence staining, we used the following antibodies: mouse anti-p34-Arc (Dubois *et al*, 2005) (undiluted), mouse anti-tubulin (Sigma T9026), rabbit anti-pericentrin (ab4448), Phalloidin-FITC (P5282) and Alexa-647 phalloidin (Fluka-65906). For inhibition experiments on isolated centrosomes, we used rabbit anti-WASH antibodies (Derivery *et al*, 2009) (2 µg/ml) (gift Alexis).

For western blot analysis, we used rabbit anti-WASH1 (1 : 1000, ab157592, abcam), rabbit anti-WASH (1:1000; Atlas), Strumpellin (1 : 1000, ab101222, Abcam), and anti-beta-tubulin (sc-5274, Santa Cruz). Labelled anti-mouse and anti-rabbit secondary antibodies (1 : 1000) and HRP-conjugated goat IgG anti-mouse and anti-rabbit (1 : 10000) for western blot were obtained from Jackson ImmunoResearch.
Cytochalasin D and nocodazole were purchased from Sigma-Aldrich. PFA was purchased from Delta Microscopies. CK666 was purchased from Sigma-Aldrich. Alexa-647-phalloidin was purchase from Life Technologies.

Figure Legend

Figure 1 – Dynamics of actin and microtubule networks during mitotic exit

A. Maximum projection (2 *z*-slices) of HeLa cells immunostained for F-actin (Phalloidin), Tubulin, Pericentrin and DAPI at metaphase and early anaphase showing actin accumulation around centrosomes in early anaphase. Scale bar-10µm
B. Quantification of F-actin (Phalloidin) intensity around pericentrin positive centrosomes in HeLa cells immunostained as in (A), showing the increase in F-actin around centrosomes at early anaphase. Mean actin metaphase = 1 ± 0.03996, n=92, mean actin anaphase = 1.875 ± 0.08895, n=121, Student t-test, ****p<0.0001;
C. Time-lapse sequence from a representative Hela cell expressing Lifeact-GFP transiting from metaphase to anaphase, showing accumulation of actin in the presumptive centrosomal region, red arrows. Images represent 4z-projection. Scale bar-10µm.
D. Time-lapse sequence of a representative HeLa cell expressing GFP-alpha-tubulin and RFP-Lifeact transiting from metaphase to anaphase showing the changes in actin and microtubules. Images represent 4 *z*-projection of movies taken every 1min. Bottom - higher magnification view of the centrosomes C1 and C2 from time-lapse above showing a transient increase in actin around the centrosomes in early anaphase. Scale bar = 10µm, 1µm in zoom. T=0 is one frame before anaphase onset. Dotted circle shows centrosome position.
E. Integrated fluorescence intensity of GFP-alpha-tubulin and RFP-Lifeact around the centrosomes for a population of cells exiting mitosis, showing actin accumulation around the centrosomes and a simultaneous decrease in tubulin over time. N=30 centrosomes (15 cells). T=0 is one frame before anaphase onset. Graph shows mean +/- SD, values were normalized to intensity at T=0.
F. Quantification and comparison of actin (RFP-Lifeact) and tubulin (a-tubulin-GFP) fluorescence intensity around the centrosomes at metaphase (-4 to -1min), early anaphase (2-5min) and late anaphase (7-10min) for a population of cells. Mean actin intensity at Metaphase =1.002 ± 0.0239, n=97, Early Anaphase = 1.023 ± 0.03047, n=101, Late anaphase = 0.9703 ± 0.05004, n=98. Tubulin intensity at Metaphase = 1.008 ± 0.03356, n=106, Early anaphase = 0.9748 ± 0.04124, n=116, Late anaphase = 0.9276 ± 0.05382, n=101, One-way ANOVA.

Figure 2 – Actin dynamics during forced mitotic exit

A. Stills from time-lapse of HeLa cells expressing GFP-alpha-tubulin and RFP-lifeact arrested at prometaphase with STLC (t=0) and forced to exit mitosis with Cdk1 inhibition (Ro3306) imaged every 90 seconds. Scale bar = 10µm and for zoom = 4µm. n = 21 cells from 4 independent experiments.
B. Quantification of actin around centrosomes when cells are forced to exit mitosis using Cdk1 inhibition as in (A), showing a similar accumulation of actin as observed in bipolar divisions. Graph shows mean actin accumulation normalized to t=0, errors bars indicate standard deviation.

C. HeLa cells expressing GFP-centrin1 arrested at prometaphase or forced mitotic exit (Ro3306 5') and stained with phalloidin. Scale bar- 5µm and for zoom-2µm.
D. The level of actin around the centrosome in (C) was quantified and normalised relative to metaphase and shows an increase during forced mitotic exit. STLC arrest 1 ± 0.01317, n=210, STLC+Ro-5mins=1.251 ± 0.02441, n=144, Unpaired t-test with Welch correction, ****p<0.0001.
E. Quantification of tubulin intensity around centrosomes during prometaphase arrested cells or cells forced to exit with Cdk1 inhibitor. Tubulin intensity decreses during forced mitotic exit. STLC-DMSO- 1 ± 0.02407, n=180, STLC-RO-3306-0.6516 ± 0.02337, n=136. P<0.0001, Welch's t test.

Figure 3 - Arp2/3 dependent actin accumulation at the centrosome.

A. Maximum projection (2-z slices) view of Hela cells pre-treated with DMSO and 0.2mM CK666 for 15 mins during their mitotic exit showing that treatment with CK666 leads to reduced accumulation of actin around the centrosomes during anaphase. Scale bar-10µm.

B. Quantification of actin around centrosomes for cells treated with DMSO or 0.2mM CK666, showing the reduction in actin accumulation around the centrosomes following CK666 treatment. DMSO-metaphase-1±0.4325, n=54, CK666-metaphase-0.936±0.4604, n=43, DMSO-anaphase-1.8±0.9736, n=76, CK666-anaphase-1.087±0.4597, n=73; one-way ANOVA, p<0.0001. Date pooled from 3 independent experiments.

C. *Z*-projection of HeLa cells expressing GFP-centrin1 pre-treated with DMSO or 0.2mM CK666 during prometaphase arrest and forced mitotic exit and stained with phalloidin for F-actin.
D. Quantification of the level of actin around the centrosome from (C), which shows the reduction in actin accumulation around centrosomes following CK666 pre-treatment. DMSO-STLC= 1 ± 0.02768, n=99, CK666 STLC= 0.776 ± 0.02186, n=87, DMSO-RO-3306= 1.339 ± 0.03048, n=127, CK666-RO-3306= 0.7699 ± 0.02246, n=70, one-way ANOVA, p<0.0001.

E. Quantification of tubulin around centrosomes for cells treated with DMSO or 0.2mM CK666, showing the failure to reduce tubulin density around centrosomes following CK666 treatment during bipolar exit. DMSO-metaphase-1±0.1968, n=54, DMSO-anaphase-0.867±0.2345, n=78, CK666-metaphase-0.7995±0.1275, n=43, CK666-anaphase-0.7407±0.1859, n=74; one-way ANOVA, p<0.0001. Data pooled from 3 independent experiments. Error bars indicated standard deviation.

F. Quantification of tubulin around centrosomes for cells treated with DMSO or 0.2mM CK666, during monopolar exit, showing the failure to reduce tubulin density around centrosomes following CK666 treatment. Data from three independent experiments. Prometaphase arrest (p.a.) 1±0.34 , n=27; forced mitotic exit (f.m.e) 0.78±0.30, n=26; p.a. plus CK666 0.49±0.34, n=30 ; f.m.e plus CK666 0.92±0.37, n=30. One-way ANOVA with Sidak's multiple comparisons test.

Figure 4 – Arp2/3 mediated actin nucleation around centrosomes *in vitro*

A. *Z*-projection of HeLa cells expressing GFP-centrin1 immunostained for p34-Arc (sub-domain Arp2/3) following prometaphase arrest and forced mitotic exit for 5min. N=3 independent experiments. Scale bar = 10µm and for zoom 2µm.
B. Levels of p34-Arc around the centrosome (3um area) were quantified relative to metaphase and increase during forced mitotic exit. STLC arrested = 1 ± 0.01576, n=153, STLC+RO-3306= 1.268 ± 0.01748, n=191, ****p<0.0001, Unpaired t-test with Welch correction. Error bars represent standard deviation.
C. *Z*-projection of centrosomes isolated from cells expressing GFP-centrin1 during prometaphase arrest and forced exit, which were immunostained with p34-Arc. N=2 independent experiments. Scale bar = 2µm.
D. Quantification of p34-Arc levels around the centrosome in (C), relative to metaphase, showing its increase during forced exit. STLC arrested = 1 ± 0.00779, n=93, STLC+RO-3306= 1.249 ± 0.02446, n=134, ****p<0.0001, Unpaired t-test with Welch correction. Error bars represent standard deviation.
E. Time-lapse of *in vitro* assay on centrosomes isolated from prometaphase arrested and cells forced to exit mitosis showing centrosomal actin nucleation over time. Scale bar = 10µm
F. Quantification of actin nucleation from isolated centrosomes as in (E) over an area of 2 µm, (white circle), showing an increase in actin nucleation around centrosomes isolated from cells undergoing forced mitotic exit. N=2 isolations, 5 independent experiments, n=16 STLC and n=19 STLC RO.
G. Color switch experiment using green- and red-labelled actin. Red actin was used first, followed by Capping protein, then green-labelled actin. The accumulation of green in the centre indicates that actin is nucleated at the centrosome. Scale bar = 10µm.
H. Quantification of (G) over the time. N=2 isolations, 2 independent experiments, n=19 STLC and n=14 STLC RO. Error bars represent standard deviation.
I. Time-lapse showing cytoplasmic actin filament formation at centrosomes isolated from cells undergoing forced exit when pre-treated with DMSO or CK666. Scale bar = 10µm.
J. Quantification of (I), showing that centrosomal actin nucleation fails when centrosomes isolated from cells undergoing exit are pre-treated with CK666. N=2 isolations, 2 independent experiments, n = 17 DMSO, 26 Ro CK666 24 STLC DMSO, 23 STLC CK666. Error bars represent standard deviation.

Figure 5 – Localization and post-translational modifications of WASH1 during mitosis

A. Phos-tag Western blot of MCF7-Her2-18 cells synchronised into distinct phases of the cell cycle showing the phospho-shift in WASH1 during mitosis.
B. Blue native PAGE Western blot showing shift in the size of WASH1 protein complex isolated from STLC treated prometaphase arrested cells when compared to cells forced to exit mitosis following Ro3306 treatment.

Figure 6 - Anaphase centrosomal actin aster formation depends on the Arp2/3 activator WASH1

A. Time-lapse of HeLa cells expressing GFP-alpha tubulin and RFP-lifeact treated with control siRNA or siRNA against WASH1 for 48 hours arrested at prometaphase and forced to exit mitosis with Ro3306 addition (t=0). Scale bar = 5µm.
B. Quantification of actin around the centrosome in (A), showing the failure to accumulate actin around the centrosome in siWASH. N = 4 experiments. Error bars represent standard deviation.

C. Western blots of lysates from cells treated with siRNA control and siRNA against WASH1 probed with WASH1 antibody, showing the reduction in WASH levels following treatment of cells with siRNA against WASH. Scale bar = 5µm and 2µm in zoom.
D. *Z*-projection of HeLa cells expressing GFP-centrin1 treated with control siRNA or siRNA against WASH, arrested at prometaphase or forced to exit mitosis and immunostained with phalloidin. Scale bar-5µm
E. Quantification of actin around the centrosome in (F), showing the failure to accumulated actin around the centrosome during forced exit in cells treated with siRNA against WASH. siControl-STLC= 1 ± 0.0189, n=165, siWASH-STLC=0.9138 ± 0.0298, n=118, siControl-STLC+RO-3306=1.911 ± 0.06221, n=147, siWASH-STLC+RO-3306=1.103 ± 0.0301, n=140. Error bars represent standard deviation. P<0.0001, one-way ANOVA.

F. Time-lapse from in vitro assay with centrosomes isolated from cells undergoing forced exit were pre-treated with either no antibody or anti-WASH1 antibody for 1 hour. Scale bar- 10µm
G. Quantification of in vitro assay from (F), showing the reduction in actin nucleation around centrosomes when they are pre-treated with anti-WASH1. Error bars represent standard deviation. 2 independent experiments.

Figure Legend for EV figures-

Figure EV1- Actin dynamics during mitotic exit in fixed cells

A. Schematic representation of metaphase and anaphase cell explaining the pools of actin measured in fixed cells. 1 and 2 refer to centrosomal actin, while regions 3 and 4 measure non-centrosomal or cytoplasmic actin.
B. Quantification of tubulin intensity around pericentrin positive centrosomes in HeLa cells immunostained as in (Figure 1A), showing the decrease in tubulin intensity around centrosomes at early anaphase. Mean tubulin metaphase = 1 ± 0.02363, n=90, mean tubulin anaphase = 0.89 ± 0.02937, n=120, Student t-test, p=0.006.
C. Quantification of non-centrosomal actin during metaphase and anaphase in fixed Hela cells (as in Figure 1A-B, Scheme in EV1A), shows that there is no significant increase in the amount of cytoplasmic actin during this period. Mean actin intensity at metaphase- 1.403±0.086, n=52, mean actin intensity at anaphase- 1.574±0.08301, n=70, p=0.1567. All values were normalized to mean actin intensity around centrosomes at metaphase. Error bars indicate standard deviation.
D. Quantification of non-centrosomal actin during metaphase and early anaphase in live Hela cells (as in Figure 1D-E, Scheme EV1A), shows that there is no significant

increase in the amount of non-centrosomal actin during this period. Mean actin intensity at metaphase-0.9994 ± 0.003416, n=108 and mean actin intensity at anaphase - 1.007 ± 0.004158, n=120. p=0.1561, Welch's t-test. All values were normalized to mean actin intensity around centrosomes at metaphase. Error bars indicate standard deviation.
E. Maximum projection (2 *z*-slices) of Jurkat cells immunostained for F-actin (Phalloidin), Tubulin, Pericentrin and DAPI at metaphase and early anaphase showing the actin accumulation around centrosomes in early anaphase. Scale bar-10µm
F. Quantification of F-actin (Phalloidin) and tubulin intensity around pericentrin positive centrosomes in Jurkat cells immunostained as in (D), showing the increase in F-actin around centrosomes at early anaphase with a decrease in tubulin. Mean actin metaphase = 1 ± 0.03351, n=70, mean actin anaphase 1.315 ± 0.04993, n=79; Mean tubulin metaphase = 1.006 ± 0.02017, n=56, mean tubulin anaphase= 0.7905 ± 0.02144, n=78, Student t-test for both, ****p<0.0001.

Figure EV2- Actin dynamics during mitotic exit in live cells

A. Representative images of time-lapse of Hela cells imaged with siR-actin, every 1 min. Red arrows point to actin in the presumptive centrosomal region. Note that with siR-actin, this pool of actin around centrosomes persists for a longer time.
B. Representative images of time-lapse of Hela cells expressing Lifeact-GFP, imaged every 1 min. Red arrows point to presumptive centrosomal region. This reporter shows a more widespread accumulation of cytoplasmic actin, with frequent enrichment around one or both centrosomes.
C. Stills from time-lapse of Hela cells expressing Lifeact-GFP, showing actin enrichment around both centrosomes.

Figure EV3- Actin dynamics during forced exit in Hela cells

A. Stills from time-lapse of Hela cells expressing Lifeact-GFP and labelled with siR-tubulin during monopolar exit, imaged every 1.5 mins, showing actin accumulation around centrosomes.
B. High resolution image of Lifeact-GFP localization in cells arrested in prometaphase (+DMSO) or cell forced to exit with Cdk1 inhibitor, for 15 mins, showing actin accumulation around the centrosomes.

Figure EV4- Actin dynamics during forced exit in Jurkat and MAVER1 cell lines

A. Maximum projection view of Jurkat cells immunostained for F-actin (Phalloidin) and Pericentrin arrested at prometaphase with STLC and forced to exit mitosis with RO-3306 (10 mins) showing the increase in F-actin around centrosomes during forced exit. Scale bar-5µm and for zoom-1µm
B. The level of actin around the centrosome in (A) was quantified and normalised relative to metaphase and shows an increase during forced mitotic exit. STLC arrest = 1.000 ± 0.08018 N=29, STLC+RO-5mins= 1.713 ± 0.2361 N=29, Welch's t-test, p=0.0072..
C. Maximum projection image of MAVER1 cells arrested in prometaphase with STLC and forced to exit with STLC + RO-3306 addition (10 mins), immunostained with

pericentrin (for centrosomes) and Phalloidin (F-actin), showing the increase in actin around the centrosomes during the forced exit. Scale bar – 5µm
D. Quantification for MAVER1 cells stained as above, showing the increase in actin during forced mitotic exit. STLC arrested- 1.000 ± 0.08336 N=35, STLC+ Ro-5mins= 3.647 ± 0.3894 N=26, Welch's t-test, ****p<0.0001. Error bars indicate standard error of the mean.

Figure EV5- Arp2/3 dependent actin nucleation around centrosomes during monopolar exit

A. Representative image of cells arrested in prometaphase with STLC incubated for 2 hours with DMSO or 0.2mM CK666 were imaged every 90 seconds as they were forced to exit mitosis as the result of Ro3306 addition. n=26 cells (DMSO) and 27 cells (CK666) from two independent experiments. Scale bar = 5µm and for zoom 2µm.
B. Quantification of actin around centrosome for cells treated with DMSO or 0.2mM CK666 prior to forced exit, shows that pre-treatment with 0.2mM CK666 leads to a failure to accumulate actin around the centrosome during exit. n=26 cells (DMSO) and 27 cells (CK666) from two independent experiments. Error bars indicated standard deviation.
C. Quantification of tubulin around centrosomes for cells treated with DMSO or 0.2mM CK666 prior to forced exit, shows that pre-treatment with 0.2mM CK666 leads to a failure to decrease tubulin around the centrosome during exit. n=26 cells (DMSO) and 27 cells (CK666) from two independent experiments. Error bars indicated standard deviation.

Figure EV6- Arp2/3 dependent actin nucleation around centrosomes during bipolar exit.

A. Maximum projection (2-z slices) view of Hela cells pre-treated with DMSO and 0.2mM CK666 for 15 mins during their mitotic exit showing that treatment with CK666 leads to a failure to decrease tubulin during anaphase. Scale bar-10µm.

B. Maximum projection view of Hela cells pre-treated with DMSO and 0.2mM CK666 during monopolar exit showing that treatment with CK666 leads to a failure to decrease tubulin during anaphase. Scale bar-10µm.

Figure EV7- Localisation of Arp2 and WASH during mitotic exit

A-B. Representative image of Hela cell expressing Centrin1-GFP in metaphase (A,A') and anaphase (B,B') immunostained for Arp2, showing increased centrosomal Arp2 localization at anaphase. Scale bar- 10µm, zoom- 1µm.
C.Maximum projection view of MAVER1 cells immunostained with WASH1 along with Pericentrin (for centrosomes) and Hoechst, in STLC treated prometaphase arrested cells and STLC+ RO-3306 treated cells, showing the localization of WASH around centrosomes during these stages. Scale bar- 5µm

REFERENCES

Akhmanova A & Steinmetz MO (2015) Control of microtubule organization and dynamics: two ends in the limelight. *Nat. Rev. Mol. Cell Biol.* **16:** 711–26

Almo SC, Pollard TD, Way M & Lattman EE (1994) Purification, characterization and crystallization of Acanthamoeba profilin expressed in Escherichia coli. *J. Mol. Biol.* **236:** 950–952

Basant A & Glotzer M (2018) Spatiotemporal Regulation of RhoA during Cytokinesis. *Curr. Biol.* **28:** R570–R580

Bastos RN, Penate X, Bates M, Hammond D & Barr FA (2012) CYK4 inhibits Rac1-dependent PAK1 and ARHGEF7 effector pathways during cytokinesis. *J. Cell Biol.* **198:** 865–880

Bettencourt-Dias M & Glover DM (2007) Centrosome biogenesis and function: centrosomics brings new understanding. *Nat. Rev. Mol. Cell Biol.* **8:** 451–463

Bovellan M, Romeo Y, Biro M, Boden A, Chugh P, Yonis A, Vaghela M, Fritzsche M, Moulding D, Thorogate R, Jégou A, Thrasher AJ, Romet-Lemonne G, Roux PP, Paluch EK & Charras G (2014) Cellular Control of Cortical Actin Nucleation. *Curr. Biol.* **24:** 1628–1635

Brangwynne CP, MacKintosh FC, Kumar S, Geisse NA, Talbot J, Mahadevan L, Parker KK, Ingber DE & Weitz DA (2006) Microtubules can bear enhanced compressive loads in living cells because of lateral reinforcement. *J. Cell Biol.* **173:** 733–741

Cao J, Crest J, Fasulo B & Sullivan W (2010) Cortical Actin Dynamics Facilitate Early-Stage Centrosome Separation. *Curr. Biol.* **20:** 770–776

Centonze VE & Borisy GG (1990) Nucleation of microtubules from mitotic centrosomes is modulated by a phosphorylated epitope. *J. Cell Sci.* **95 (Pt 3):** 405–11

Chaigne A, Campillo C, Voituriez R, Gov NS, Sykes C, Verlhac M-H & Terret M-E (2016) F-actin mechanics control spindle centring in the mouse zygote. *Nat. Commun.* **7:** 10253

Chugh P, Clark AG, Smith MB, Cassani DAD, Dierkes K, Ragab A, Roux PP, Charras G, Salbreux G & Paluch EK (2017) Actin cortex architecture regulates cell surface tension. *Nat. Cell Biol.* **19:** 689–697

Clark AG, Dierkes K & Paluch EK (2013) Monitoring Actin Cortex Thickness in Live Cells. *Biophys. J.* **105:** 570–580

Coles CH & Bradke F (2015) Coordinating neuronal actin-microtubule dynamics. *Curr. Biol.* **25:** R677-91

Colin A, Singaravelu P, Théry M, Blanchoin L & Gueroui Z (2018) Actin-Network Architecture Regulates Microtubule Dynamics. *Curr. Biol.* **28:** 2647–2656.e4

von Dassow G (2009) Concurrent cues for cytokinetic furrow induction in animal cells. *Trends Cell Biol.* **19:** 165–173

DeBonis S, Skoufias DA, Lebeau L, Lopez R, Robin G, Margolis RL, Wade RH & Kozielski F (2004) In vitro screening for inhibitors of the human mitotic kinesin Eg5 with antimitotic and antitumor activities. *Mol. Cancer Ther.* **3:** 1079–90

Derivery E, Sousa C, Gautier JJ, Lombard B, Loew D & Gautreau A (2009) The Arp2/3 Activator WASH Controls the Fission of Endosomes through a Large Multiprotein Complex. *Dev. Cell* **17:** 712–723

Dix CL, Matthews HK, Uroz M, McLaren S, Wolf L, Heatley N, Win Z, Almada P, Henriques R, Boutros M, Trepat X & Baum B (2018) The Role of Mitotic Cell-Substrate Adhesion Re-modeling in Animal Cell Division. *Dev. Cell* **45:** 132–

145.e3
Dubois T, Paléotti O, Mironov A a, Fraisier V, Stradal TEB, De Matteis MA, Franco M & Chavrier P (2005) Golgi-localized GAP for Cdc42 functions downstream of ARF1 to control Arp2/3 complex and F-actin dynamics. *Nat. Cell Biol.* **7:** 353–64
Egile C, Loisel TP, Laurent V, Li R, Pantaloni D, Sansonetti PJ & Carlier M (1999) Activation of the CDC42 Effector N-WASP by the Shigella flexneri IcsA Protein Promotes Actin Nucleation by Arp2/3 Complex and Bacterial Actin-based Motility. *J. Cell Biol.* **146:** 1319–1332
Elie A, Prezel E, Guérin C, Denarier E, Ramirez-Rios S, Serre L, Andrieux A, Fourest-Lieuvin A, Blanchoin L & Arnal I (2015) Tau co-organizes dynamic microtubule and actin networks. *Sci. Rep.* **5:** 9964
Fakhri N, Wessel AD, Willms C, Pasquali M, Klopfenstein DR, MacKintosh FC & Schmidt CF (2014) High-resolution mapping of intracellular fluctuations using carbon nanotubes. *Science* **344:** 1031–5
Falck S, Paavilainen VO, Wear M a, Grossmann JG, Cooper J a & Lappalainen P (2004) Biological role and structural mechanism of twinfilin-capping protein interaction. *EMBO J.* **23:** 3010–3019
Farina F, Gaillard J, Guérin C, Couté Y, Sillibourne J, Blanchoin L & Théry M (2016) The centrosome is an actin-organizing centre. *Nat. Cell Biol.* **18:** 65–75
Fededa JP & Gerlich DW (2012) Molecular control of animal cell cytokinesis. *Nat. Cell Biol.* **14:** 440–447
Ferreira JG, Pereira AJ, Akhmanova A & Maiato H (2013) Aurora B spatially regulates EB3 phosphorylation to coordinate daughter cell adhesion with cytokinesis. *J. Cell Biol.* **201:** 709–724
Field CM & Lénárt P (2011) Bulk Cytoplasmic Actin and Its Functions in Meiosis and Mitosis. *Curr. Biol.* **21:** R825–R830
Fink J, Carpi N, Betz T, Bétard A, Chebah M, Azioune A, Bornens M, Sykes C, Fetler L, Cuvelier D & Piel M (2011) External forces control mitotic spindle positioning. *Nat. Cell Biol.* **13:** 771–778
Fischer-Friedrich E, Hyman AA, Jülicher F, Müller DJ & Helenius J (2015) Quantification of surface tension and internal pressure generated by single mitotic cells. *Sci. Rep.* **4:** 6213
Gupton SL, Salmon WC & Waterman-Storer CM (2002) Converging populations of f-actin promote breakage of associated microtubules to spatially regulate microtubule turnover in migrating cells. *Curr. Biol.* **12:** 1891–9
Hu C-K, Coughlin M, Field CM & Mitchison TJ (2008) Cell polarization during monopolar cytokinesis. *J. Cell Biol.* **181:** 195–202
Huber F, Boire A, López MP & Koenderink GH (2015) Cytoskeletal crosstalk: when three different personalities team up. *Curr. Opin. Cell Biol.* **32:** 39–47
Hutchins BI & Wray S (2014) Capture of microtubule plus-ends at the actin cortex promotes axophilic neuronal migration by enhancing microtubule tension in the leading process. *Front. Cell. Neurosci.* **8:** 400
Hyman A, Drechsel D, Kellogg D, Salser S, Sawin K, Steffen P, Wordeman L & Mitchison T (1991) Preparation of modified tubulins. *Methods Enzymol.* **196:** 478–85
Ibarra N, Pollitt A & Insall RH (2005) Regulation of actin assembly by SCAR/WAVE proteins. *Biochem. Soc. Trans.* **33:** 1243
Inoue D, Obino D, Pineau J, Farina F, Gaillard J, Guerin C, Blanchoin L, Lennon-Duménil A & Théry M (2019) Actin filaments regulate microtubule growth at the centrosome. *EMBO J.***:** e99630

Isambert H, Venir P, Maggs anthony C, Fattoum A, Kassab R, Pantaloni D & Carlier M-F (1995) Flexibility of actin filaments derived from thermal fluctuations. Effect of bound nucleotide, phalloidin, and muscle regulatory proteins. *J. Biol. Chem.* **270:** 11437–11444

Karayel Ö, Şanal E, Giese SH, Üretmen Kagıalı ZC, Polat AN, Hu C-K, Renard BY, Tuncbag N & Özlü N (2018) Comparative phosphoproteomic analysis reveals signaling networks regulating monopolar and bipolar cytokinesis. *Sci. Rep.* **8:** 2269

Katrukha EA, Mikhaylova M, van Brakel HX, van Bergen En Henegouwen PM, Akhmanova A, Hoogenraad CC & Kapitein LC (2017) Probing cytoskeletal modulation of passive and active intracellular dynamics using nanobody-functionalized quantum dots. *Nat. Commun.* **8:** 14772

Kaur S, Fielding AB, Gassner G, Carter NJ & Royle SJ (2014) An unmet actin requirement explains the mitotic inhibition of clathrin-mediated endocytosis. *Elife* **3:**

Kaverina I, Rottner K & Small J V (1998) Targeting, capture, and stabilization of microtubules at early focal adhesions. *J. Cell Biol.* **142:** 181–90

Khodjakov A & Rieder CL (1999) The sudden recruitment of gamma-tubulin to the centrosome at the onset of mitosis and its dynamic exchange throughout the cell cycle, do not require microtubules. *J. Cell Biol.* **146:** 585–96

King JS, Veltman DM, Georgiou M, Baum B & Insall RH (2010) SCAR/WAVE is activated at mitosis and drives myosin-independent cytokinesis. *J. Cell Sci.* **123:** 2246–55

Kiyomitsu T & Cheeseman IM (2013) Cortical Dynein and Asymmetric Membrane Elongation Coordinately Position the Spindle in Anaphase. *Cell* **154:** 391–402

Lancaster OM, Le Berre M, Dimitracopoulos A, Bonazzi D, Zlotek-Zlotkiewicz E, Picone R, Duke T, Piel M & Baum B (2013) Mitotic Rounding Alters Cell Geometry to Ensure Efficient Bipolar Spindle Formation. *Dev. Cell* **25:** 270–283

Lock JG, Jones MC, Askari JA, Gong X, Oddone A, Olofsson H, Göransson S, Lakadamyali M, Humphries MJ & Strömblad S (2018) Reticular adhesions are a distinct class of cell-matrix adhesions that mediate attachment during mitosis. *Nat. Cell Biol.* **20:** 1290–1302

López MP, Huber F, Grigoriev I, Steinmetz MO, Akhmanova A, Koenderink GH & Dogterom M (2014) Actin–microtubule coordination at growing microtubule ends. *Nat. Commun.* **5:** 4778

Luo T, Srivastava V, Ren Y & Robinson DN (2014) Mimicking the mechanical properties of the cell cortex by the self-assembly of an actin cortex in vesicles. *Appl. Phys. Lett.* **104:** 153701

Machesky LM, Mullins RD, Higgs HN, Kaiser D a, Blanchoin L, May RC, Hall ME & Pollard TD (1999) Scar, a WASp-related protein, activates nucleation of actin filaments by the Arp2/3 complex. *Proc. Natl. Acad. Sci. U. S. A.* **96:** 3739–3744

MacLean-Fletcher S & Pollard TD (1980) Identification of a factor in conventional muscle actin preparations which inhibits actin filament self-association. *Biochem. Biophys. Res. Commun.* **96:** 18–27

Maddox AS & Burridge K (2003) RhoA is required for cortical retraction and rigidity during mitotic cell rounding. *J. Cell Biol.* **160:** 255–65

Magidson V, O'Connell CB, Lončarek J, Paul R, Mogilner A & Khodjakov A (2011) The Spatial Arrangement of Chromosomes during Prometaphase Facilitates Spindle Assembly. *Cell* **146:** 555–567

Matthews HK, Delabre U, Rohn JL, Guck J, Kunda P & Baum B (2012) Changes in

Ect2 Localization Couple Actomyosin-Dependent Cell Shape Changes to Mitotic Progression. *Dev. Cell* **23:** 371–383
Mayer TU, Kapoor TM, Haggarty SJ, King RW, Schreiber SL & Mitchison TJ (1999) Small molecule inhibitor of mitotic spindle bipolarity identified in a phenotype-based screen. *Science* **286:** 971–4
Mchedlishvili N, Matthews HK, Corrigan A & Baum B (2018) Two-step interphase microtubule disassembly aids spindle morphogenesis. *BMC Biol.* **16:** 14
McNally FJ (2013) Mechanisms of spindle positioning. *J. Cell Biol.* **200:** 131–140
Meraldi P & Nigg EA (2002) The centrosome cycle. *FEBS Lett.* **521:** 9–13
Michelot A, Berro J, Guérin C, Boujemaa-Paterski R, Staiger CJ, Martiel J-L & Blanchoin L (2007) Actin-filament stochastic dynamics mediated by ADF/cofilin. *Curr. Biol.* **17:** 825–33
Mitchison TJ & Kirschner MW (1985) Properties of the kinetochore in vitro. II. Microtubule capture and ATP-dependent translocation. *J. Cell Biol.* **101:** 766–77
Mitsushima M, Aoki K, Ebisuya M, Matsumura S, Yamamoto T, Matsuda M, Toyoshima F & Nishida E (2010) Revolving movement of a dynamic cluster of actin filaments during mitosis. *J. Cell Biol.* **191:** 453–462
Mohan R & John A (2015) Microtubule-associated proteins as direct crosslinkers of actin filaments and microtubules. *IUBMB Life* **67:** 395–403
Motegi F, Velarde N V., Piano F & Sugimoto A (2006) Two Phases of Astral Microtubule Activity during Cytokinesis in C. elegans Embryos. *Dev. Cell* **10:** 509–520
Moulding DA, Moeendarbary E, Valon L, Record J, Charras GT & Thrasher AJ (2012) Excess F-actin mechanically impedes mitosis leading to cytokinesis failure in X-linked neutropenia by exceeding Aurora B kinase error correction capacity. *Blood* **120:** 3803–3811
Neujahr R, Heizer C & Gerisch G (1997) Myosin II-independent processes in mitotic cells of Dictyostelium discoideum: redistribution of the nuclei, re-arrangement of the actin system and formation of the cleavage furrow. *J. Cell Sci.* **110 (Pt 2):** 123–37
Nezis IP, Sagona AP, Schink KO & Stenmark H (2010) Divide and ProsPer: The emerging role of PtdIns3P in cytokinesis. *Trends Cell Biol.* **20:** 642–649
Niethammer P, Kronja I, Kandels-Lewis S, Rybina S, Bastiaens P & Karsenti E (2007) Discrete states of a protein interaction network govern interphase and mitotic microtubule dynamics. *PLoS Biol.* **5:** e29
Obino D, Farina F, Malbec O, Sáez PJ, Maurin M, Gaillard J, Dingli F, Loew D, Gautreau A, Yuseff M-I, Blanchoin L, Théry M & Lennon-Duménil A-M (2016) Actin nucleation at the centrosome controls lymphocyte polarity. *Nat. Commun.* **7:** 10969
Olsen J V., Vermeulen M, Santamaria A, Kumar C, Miller ML, Jensen LJ, Gnad F, Cox J, Jensen TS, Nigg EA, Brunak S & Mann M (2010) Quantitative Phosphoproteomics Reveals Widespread Full Phosphorylation Site Occupancy During Mitosis. *Sci. Signal.* **3:** ra3-ra3
Piehl M, Tulu US, Wadsworth P & Cassimeris L (2004) Centrosome maturation: Measurement of microtubule nucleation throughout the cell cycle by using GFP-tagged EB1. *Proc. Natl. Acad. Sci.* **101:** 1584–1588
Piel M, Nordberg J, Euteneuer U & Bornens M (2001) Centrosome-dependent exit of cytokinesis in animal cells. *Science* **291:** 1550–3
Po'uha ST & Kavallaris M (2015) Gamma-actin is involved in regulating centrosome function and mitotic progression in cancer cells. *Cell Cycle* **14:** 3908–3919

Pollard TD, Blanchoin L & Mullins RD (2000) Molecular Mechanisms Controlling Actin Filament Dynamics in Nonmuscle Cells. *Annu. Rev. Biophys. Biomol. Struct.* **29:** 545–576

Pollard TD & Borisy GG (2003) Cellular motility driven by assembly and disassembly of actin filaments. *Cell* **112:** 453–65

Ragkousi K & Gibson MC (2014) Cell division and the maintenance of epithelial order. *J. Cell Biol.* **207:** 181–188

Ramkumar N & Baum B (2016) Coupling changes in cell shape to chromosome segregation. *Nat. Rev. Mol. Cell Biol.* **17:** 511–521

Rappaport R (1996) Cytokinesis in Animal Cells Cambridge: Cambridge University Press

Reinsch S & Karsenti E (1994) Orientation of spindle axis and distribution of plasma membrane proteins during cell division in polarized MDCKII cells. *J. Cell Biol.* **126:** 1509–26

Reymann A-C, Suarez C, Guérin C, Martiel J-L, Staiger CJ, Blanchoin L & Boujemaa-Paterski R (2011) Turnover of branched actin filament networks by stochastic fragmentation with ADF/cofilin. *Mol. Biol. Cell* **22:** 2541–50

Robison P, Caporizzo MA, Ahmadzadeh H, Bogush AI, Chen CY, Margulies KB, Shenoy VB & Prosser BL (2016) Detyrosinated microtubules buckle and bear load in contracting cardiomyocytes. *Science* **352:** aaf0659

Rodrigues NTL, Lekomtsev S, Jananji S, Kriston-Vizi J, Hickson GRX & Baum B (2015) Kinetochore-localized PP1–Sds22 couples chromosome segregation to polar relaxation. *Nature* **524:** 489–492

Rodriguez OC, Schaefer AW, Mandato CA, Forscher P, Bement WM & Waterman-Storer CM (2003) Conserved microtubule–actin interactions in cell movement and morphogenesis. *Nat. Cell Biol.* **5:** 599–609

Rohn JL, Patel J V, Neumann B, Bulkescher J, Mchedlishvili N, McMullan RC, Quintero OA, Ellenberg J & Baum B (2014) Myo19 ensures symmetric partitioning of mitochondria and coupling of mitochondrial segregation to cell division. *Curr. Biol.* **24:** 2598–605

Rosa A, Vlassaks E, Pichaud F & Baum B (2015) Ect2/Pbl acts via Rho and polarity proteins to direct the assembly of an isotropic actomyosin cortex upon mitotic entry. *Dev. Cell* **32:** 604–16

Rosenblatt J, Cramer LP, Baum B & McGee KM (2004) Myosin II-dependent cortical movement is required for centrosome separation and positioning during mitotic spindle assembly. *Cell* **117:** 361–72

Sabino D, Gogendeau D, Gambarotto D, Nano M, Pennetier C, Dingli F, Arras G, Loew D & Basto R (2015) Moesin is a major regulator of centrosome behavior in epithelial cells with extra centrosomes. *Curr. Biol.* **25:** 879–89

Salmon ED & Wolniak SM (1990) Role of Microtubules in Stimulating Cytokinesis in Animal Cells. *Ann. N. Y. Acad. Sci.* **582:** 88–98

Shelanski M (1973) Chemistry of the filaments and tubules of brain. *J. Histochem. Cytochamistry* **21:** 529–539

Shi P, Wang Y, Huang Y, Zhang C, Li Y, Liu Y, Li T, Wang W, Liang X & Wu C (2019) Arp2/3-branched actin regulates microtubule acetylation levels and affects mitochondrial distribution. *J Cell Sci* **132:** jcs226506

Skoufias DA, DeBonis S, Saoudi Y, Lebeau L, Crevel I, Cross R, Wade RH, Hackney D & Kozielski F (2006) S-trityl-L-cysteine is a reversible, tight binding inhibitor of the human kinesin Eg5 that specifically blocks mitotic progression. *J. Biol. Chem.* **281:** 17559–69

Sorce B, Escobedo C, Toyoda Y, Stewart MP, Cattin CJ, Newton R, Banerjee I, Stettler A, Roska B, Eaton S, Hyman AA, Hierlemann A & Müller DJ (2015) Mitotic cells contract actomyosin cortex and generate pressure to round against or escape epithelial confinement. *Nat. Commun.* **6:** 8872

Spudich JA & Watt S (1971) The Regulation of Rabbit Skeletal Muscle Contraction. *J. Biol. Chem.* **246:** 4866–4871

Su K-C, Takaki T & Petronczki M (2011) Targeting of the RhoGEF Ect2 to the Equatorial Membrane Controls Cleavage Furrow Formation during Cytokinesis. *Dev. Cell* **21:** 1104–1115

Sulimenko V, Hájková Z, Klebanovych A & Dráber P (2017) Regulation of microtubule nucleation mediated by γ-tubulin complexes. *Protoplasma* **254:** 1187–1199

Thery M, Inoue D, Obino D, Farina F, Gaillard J, Guérin C, Blanchoin L & Lennon-Duménil A-M (2018) Actin filaments regulate microtubule growth at the centrosome. *bioRxiv***:** 302190

Thery M, Racine V, Piel M, Pepin A, Dimitrov A, Chen Y, Sibarita J-B & Bornens M (2006) Anisotropy of cell adhesive microenvironment governs cell internal organization and orientation of polarity. *Proc. Natl. Acad. Sci.* **103:** 19771–19776

Tyrrell BJ, Woodham EF, Spence HJ, Strathdee D, Insall RH & Machesky LM (2016) Loss of strumpellin in the melanocytic lineage impairs the WASH Complex but does not affect coat colour. *Pigment Cell Melanoma Res.*

Vilmos P, Kristó I, Szikora S, Jankovics F, Lukácsovich T, Kari B & Erdélyi M (2016) The actin-binding ERM protein Moesin directly regulates spindle assembly and function during mitosis. *Cell Biol. Int.* **40:** 696–707

Wagner E & Glotzer M (2016) Local RhoA activation induces cytokinetic furrows independent of spindle position and cell cycle stage. *J. Cell Biol.* **213:** 641–649

Waterman-Storer CM & Salmon ED (1997) Actomyosin-based retrograde flow of microtubules in the lamella of migrating epithelial cells influences microtubule dynamic instability and turnover and is associated with microtubule breakage and treadmilling. *J. Cell Biol.* **139:** 417–34

White EA & Glotzer M (2012) Centralspindlin: at the heart of cytokinesis. *Cytoskeleton (Hoboken).* **69:** 882–92

Wittmann T, Bokoch GM & Waterman-Storer CM (2003) Regulation of leading edge microtubule and actin dynamics downstream of Rac1. *J. Cell Biol.* **161:** 845–51

Woolner S, O'Brien LL, Wiese C & Bement WM (2008) Myosin-10 and actin filaments are essential for mitotic spindle function. *J. Cell Biol.* **182:** 77–88

Yüce Ö, Piekny A & Glotzer M (2005) An ECT2–centralspindlin complex regulates the localization and function of RhoA. *J. Cell Biol.* **170:** 571–582

Zhai Y, Kronebusch PJ, Simon PM & Borisy GG (1996) Microtubule dynamics at the G2/M transition: abrupt breakdown of cytoplasmic microtubules at nuclear envelope breakdown and implications for spindle morphogenesis. *J. Cell Biol.* **135:** 201–14

Zhang W & Robinson DN (2005) Balance of actively generated contractile and resistive forces controls cytokinesis dynamics. *Proc. Natl. Acad. Sci. U. S. A.* **102:** 7186–91

Zhou F-Q, Waterman-Storer CM & Cohan CS (2002) Focal loss of actin bundles causes microtubule redistribution and growth cone turning. *J. Cell Biol.* **157:** 839–49

Figure 1

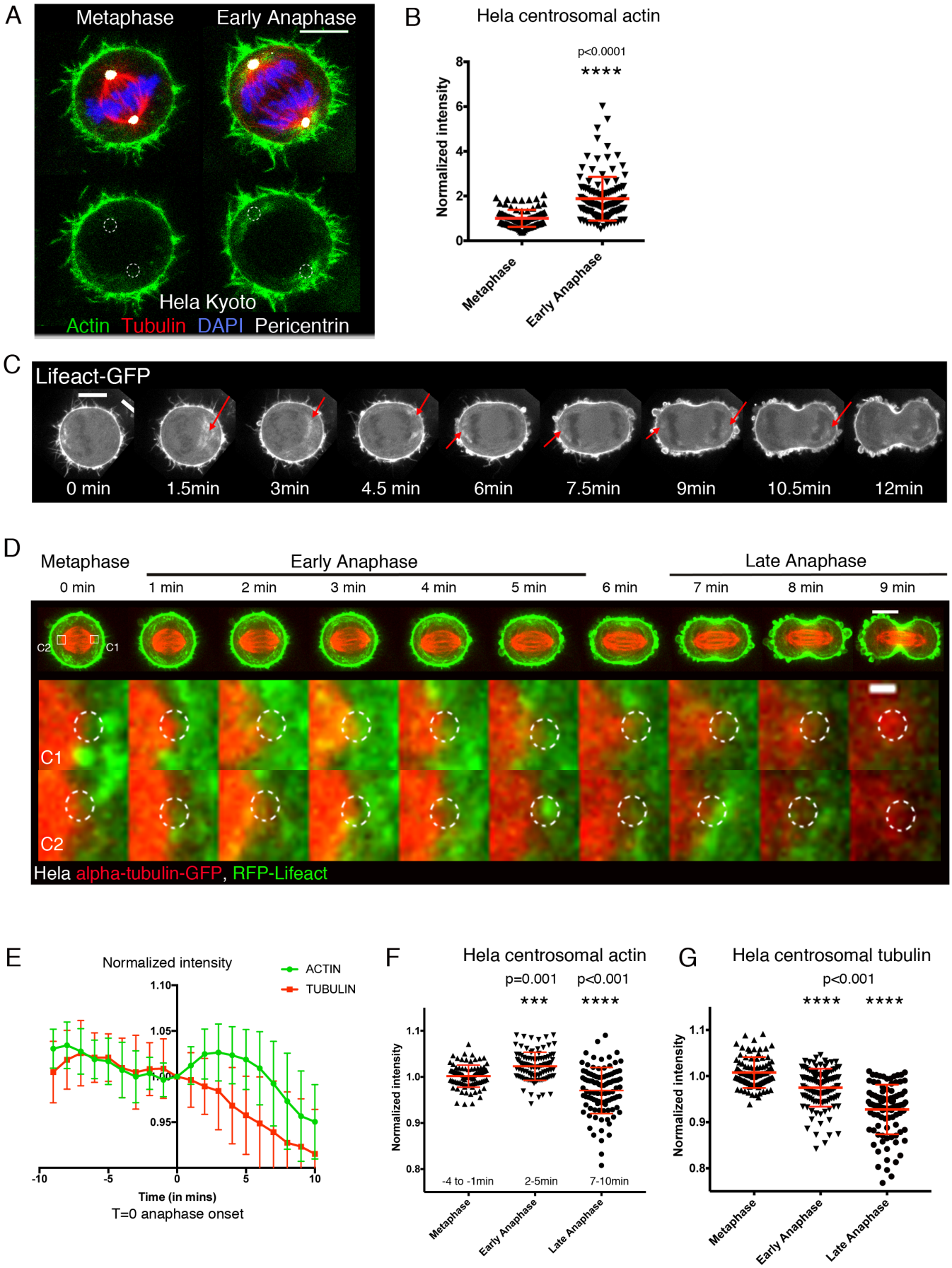
A
Metaphase
Early Anaphase
Hela Kyoto
Actin Tubulin DAPI Pericentrin
B
Hela centrosomal actin
p<0.0001
****
Normalized intensity
Metaphase
Early Anaphase
C
Lifeact-GFP
0 min
1.5min
3min
4.5 min
6min
7.5min
9min
10.5min
12min
D
Metaphase
Early Anaphase
Late Anaphase
0 min
1 min
2 min
3 min
4 min
5 min
6 min
7 min
8 min
9 min
C2
C1
C1
C2
Hela alpha-tubulin-GFP, RFP-Lifeact
E
Normalized intensity
ACTIN
TUBULIN
Time (in mins)
T=0 anaphase onset
F
Hela centrosomal actin
p=0.001
p<0.001
***
****
Normalized intensity
-4 to -1min
2-5min
7-10min
Metaphase
Early Anaphase
Late Anaphase
G
Hela centrosomal tubulin
p<0.001
****
****
Normalized intensity
Metaphase
Early Anaphase
Late Anaphase

Figure 2

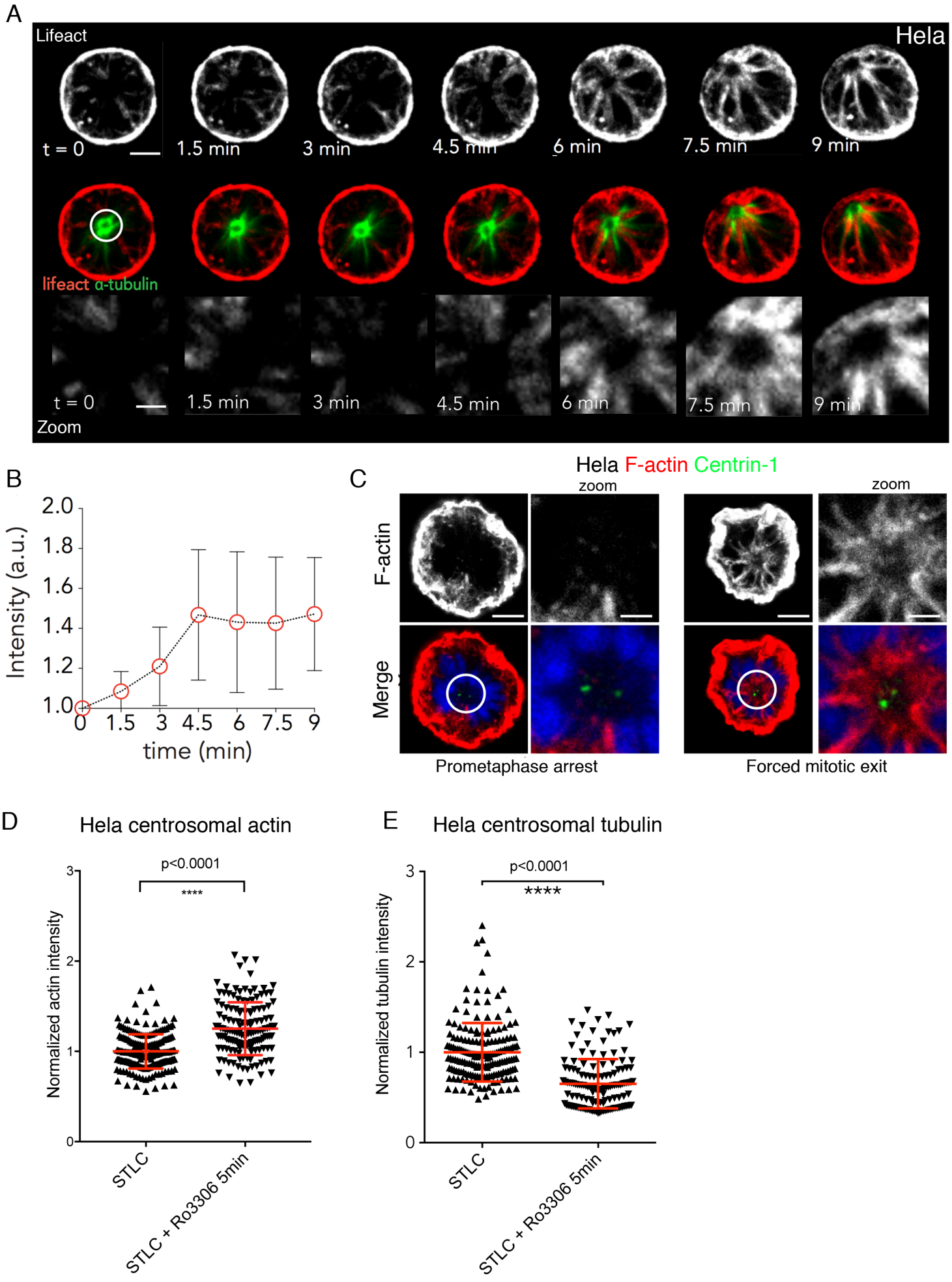
A
Lifeact
Hela
t = 0
1.5 min
3 min
4.5 min
6 min
7.5 min
9 min
lifeact α-tubulin
Zoom
B
Intensity (a.u.)
time (min)
C
Hela F-actin Centrin-1
zoom
F-actin
Merge
Prometaphase arrest
Forced mitotic exit
D
Hela centrosomal actin
p<0.0001
****
Normalized actin intensity
STLC
STLC + Ro3306 5min
E
Hela centrosomal tubulin
Normalized tubulin intensity

Figure 3

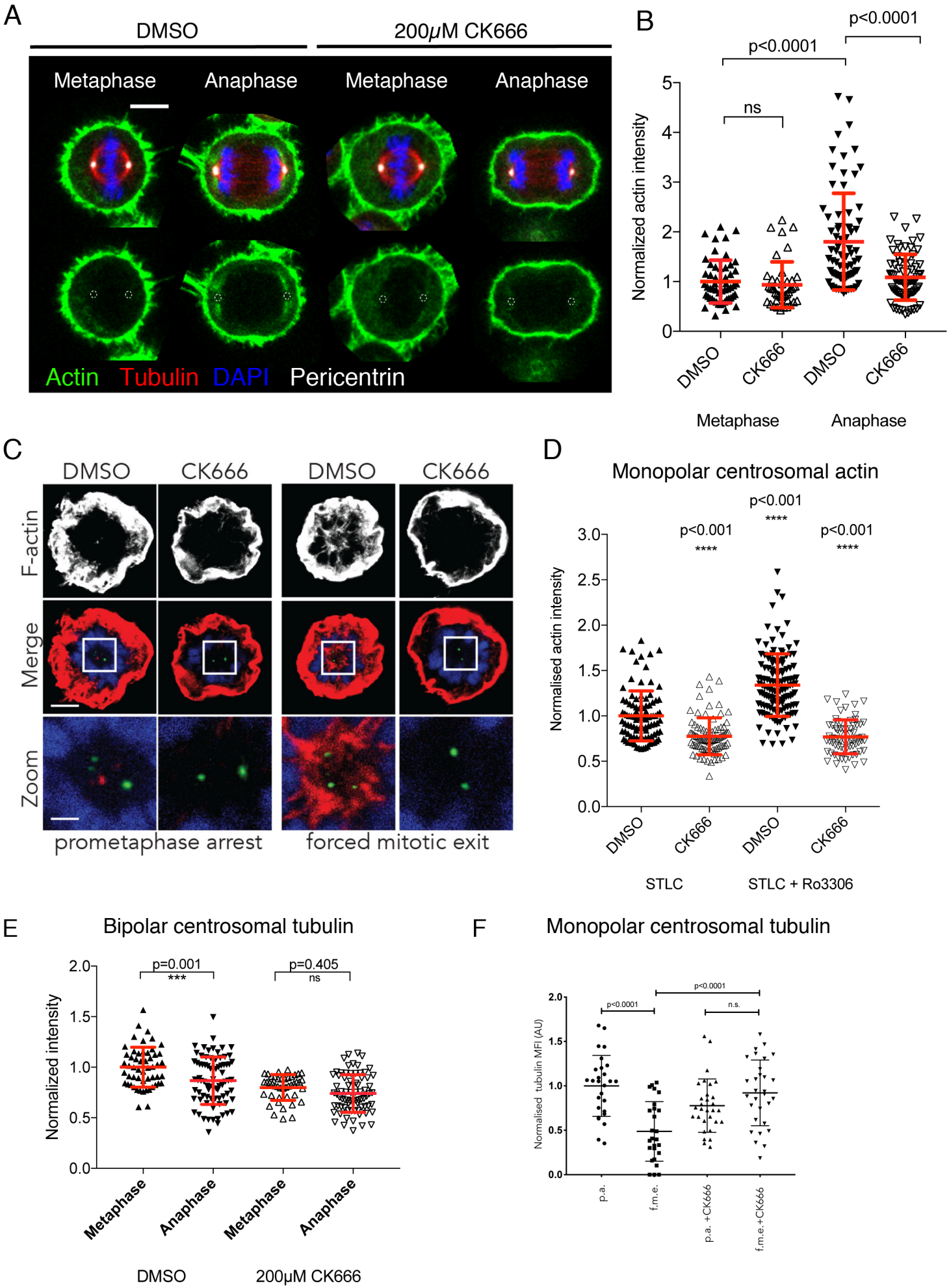
A
DMSO
200μM CK666
Metaphase
Anaphase
Metaphase
Anaphase
Actin
Tubulin
DAPI
Pericentrin
B
Bipolar centrosomal actin
p<0.0001
p<0.0001
ns
Normalized actin intensity
DMSO
CK666
DMSO
CK666
Metaphase
Anaphase
C
DMSO
CK666
DMSO
CK666
F-actin
Merge
Zoom
prometaphase arrest
forced mitotic exit
D
Monopolar centrosomal actin
p<0.001
****
p<0.001
****
p<0.001
****
Normalised actin intensity
DMSO
CK666
DMSO
CK666
STLC
STLC + Ro3306
E
Bipolar centrosomal tubulin
p=0.001
***
p=0.405
ns
Normalized intensity
Metaphase
Anaphase
Metaphase
Anaphase
DMSO
200μM CK666
F
Monopolar centrosomal tubulin
p<0.0001
p<0.0001
n.s.
Normalised tubulin MFI (AU)
p.a.
f.m.e.
p.a. +CK666
f.m.e.+CK666

Figure 4

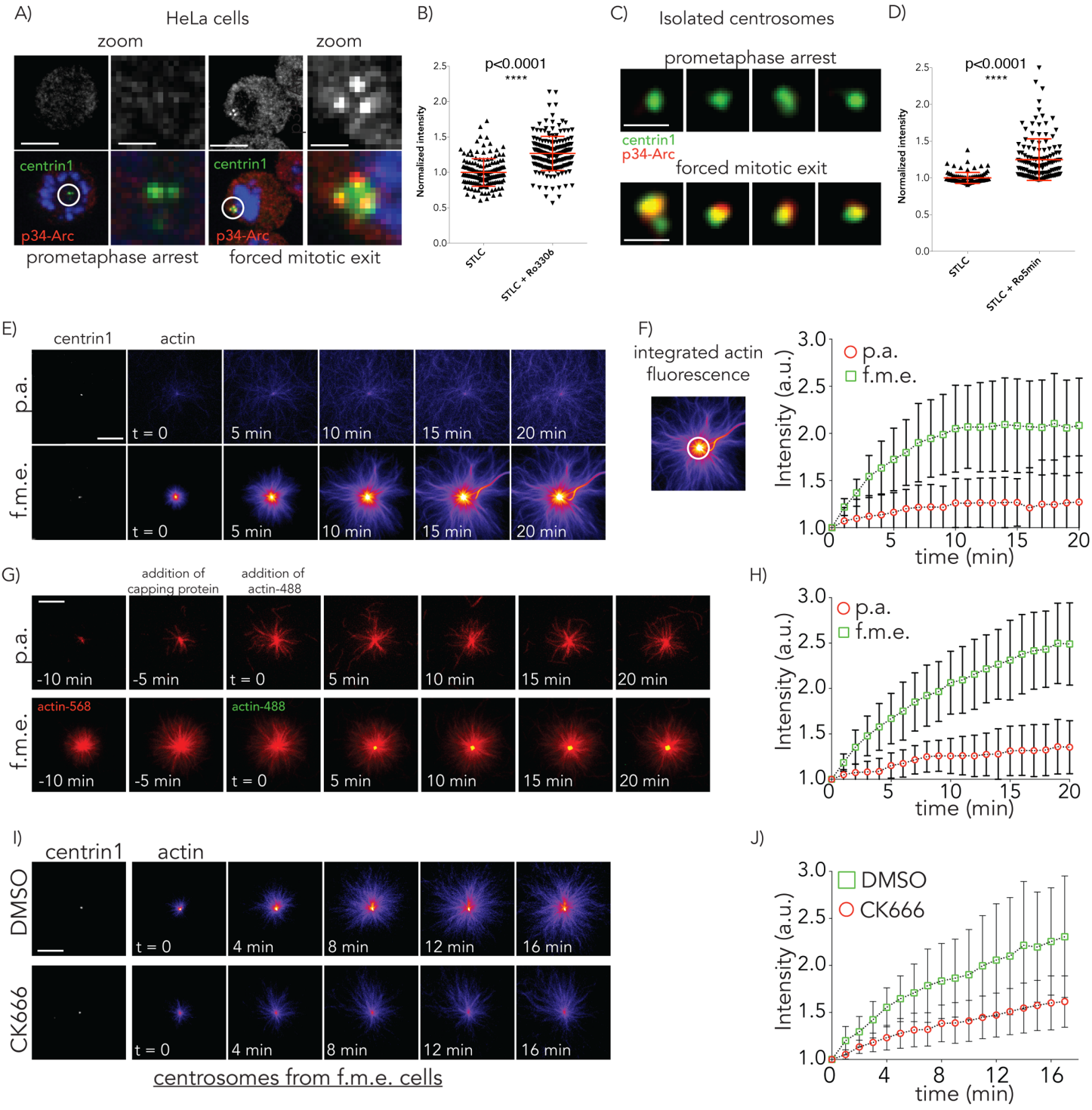
A)
HeLa cells
zoom
zoom
centrin1
p34-Arc
centrin1
p34-Arc
prometaphase arrest
forced mitotic exit
B)
p<0.0001
****
Normalized intensity
STLC
STLC + Ro3306
C)
Isolated centrosomes
prometaphase arrest
centrin1
p34-Arc
forced mitotic exit
D)
p<0.0001
****
Normalized intensity
STLC
STLC + Ro5min
E)
centrin1
actin
p.a.
f.m.e.
t = 0
5 min
10 min
15 min
20 min
F)
integrated actin fluorescence
p.a.
f.m.e.
Intensity (a.u.)
time (min)
G)
addition of capping protein
addition of actin-488
p.a.
f.m.e.
actin-568
actin-488
-10 min
-5 min
t = 0
5 min
10 min
15 min
20 min
H)
p.a.
f.m.e.
Intensity (a.u.)
time (min)
I)
centrin1
actin
DMSO
CK666
t = 0
4 min
8 min
12 min
16 min
centrosomes from f.m.e. cells
J)
DMSO
CK666
Intensity (a.u.)
time (min)

Figure 5

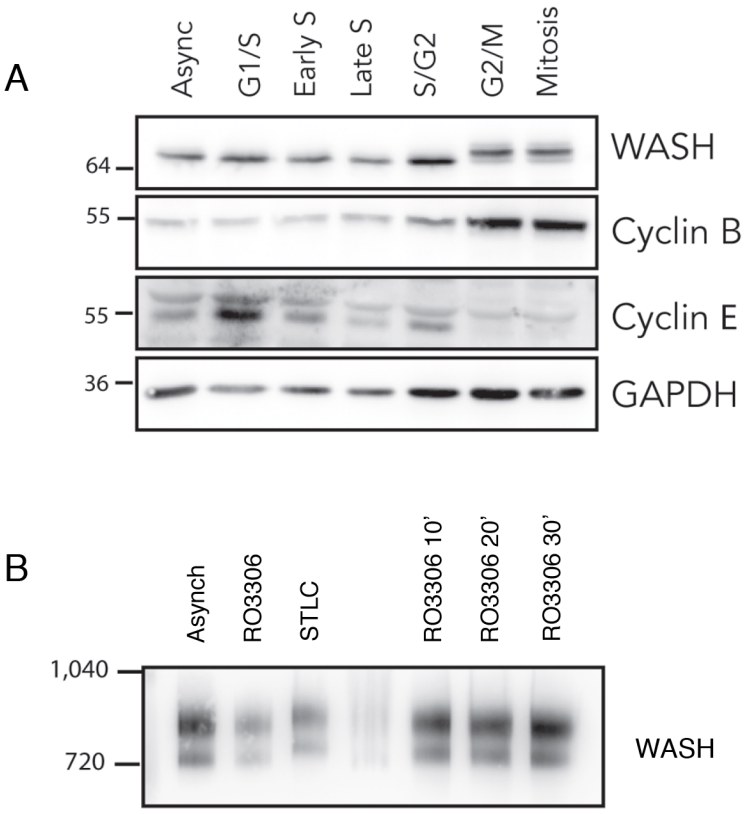
A
Async
G1/S
Early S
Late S
S/G2
G2/M
Mitosis
64
55
55
36
WASH
Cyclin B
Cyclin E
GAPDH
B
Asynch
RO3306
STLC
RO3306 10'
RO3306 20'
RO3306 30'
1,040
720
WASH

Figure 6

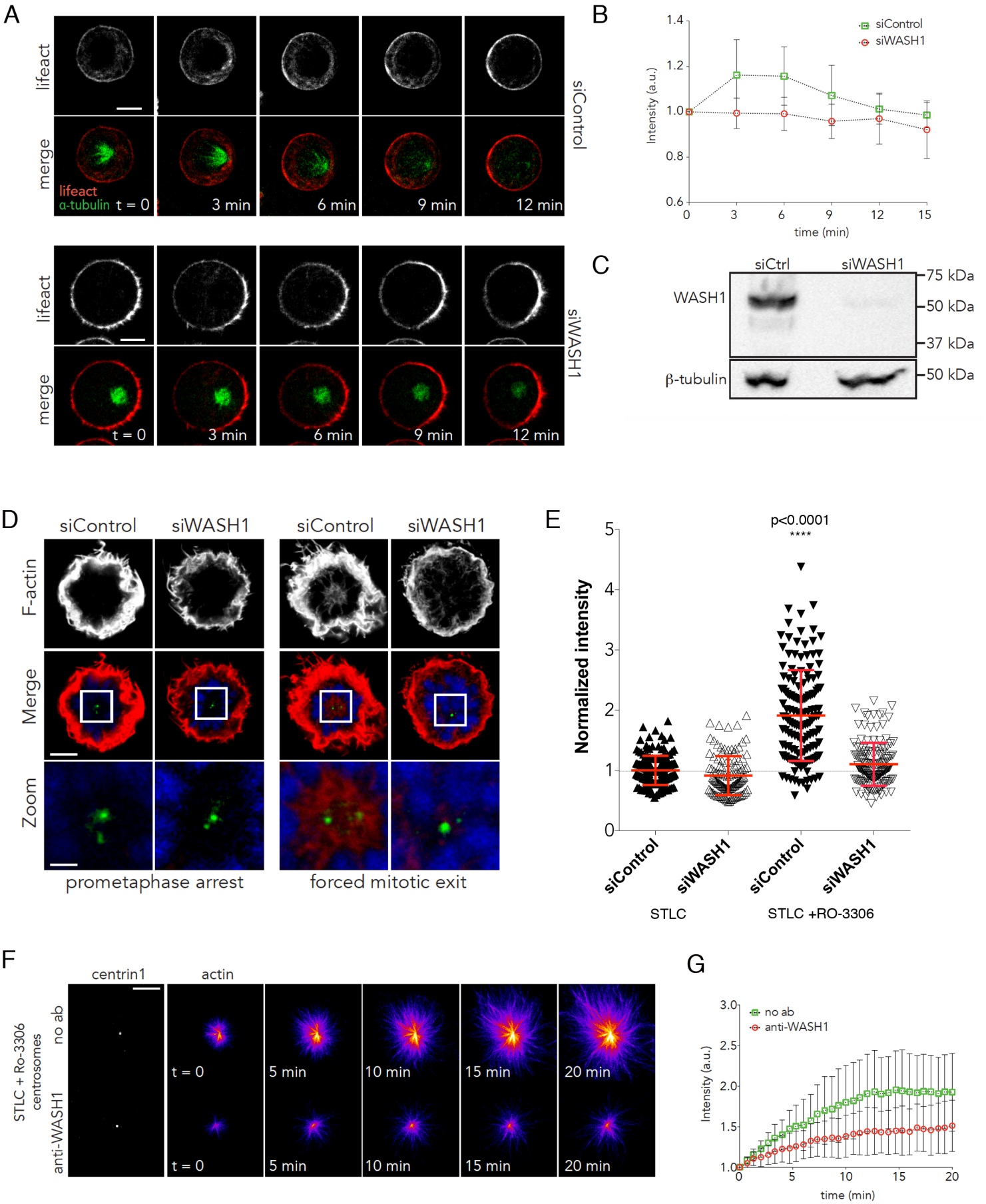
A
lifeact
merge
lifeact
α-tubulin t = 0
3 min
6 min
9 min
12 min
siControl
siWASH1
B
siControl
siWASH1
Intensity (a.u.)
time (min)
C
siCtrl
siWASH1
WASH1
β-tubulin
75 kDa
50 kDa
37 kDa
50 kDa
D
siControl
siWASH1
siControl
siWASH1
F-actin
Merge
Zoom
prometaphase arrest
forced mitotic exit
E
p<0.0001
****
Normalized intensity
siControl
siWASH1
siControl
siWASH1
STLC
STLC +RO-3306
F
centrin1
actin
STLC + Ro-3306
centrosomes
no ab
anti-WASH1
t = 0
5 min
10 min
15 min
20 min
G
no ab
anti-WASH1
Intensity (a.u.)
time (min)

Supp Figure 1

A

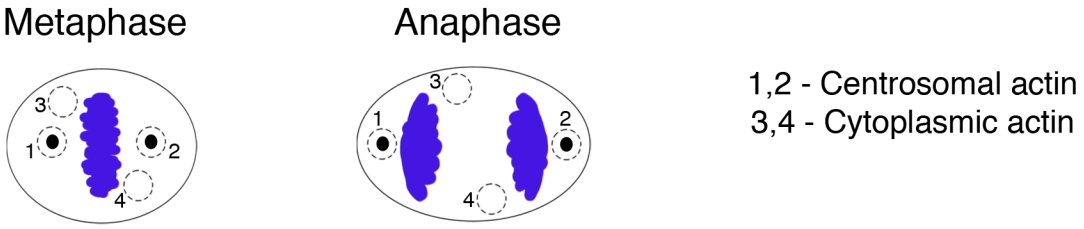

B Hela centrosomal tubulin

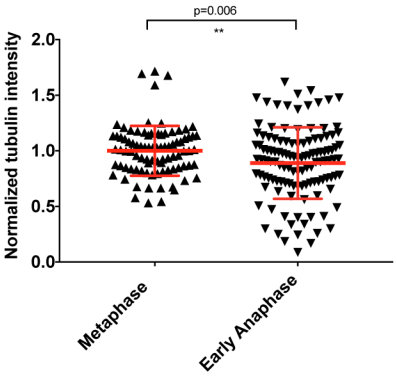

C Hela cytoplasmic actin (Fixed cells)

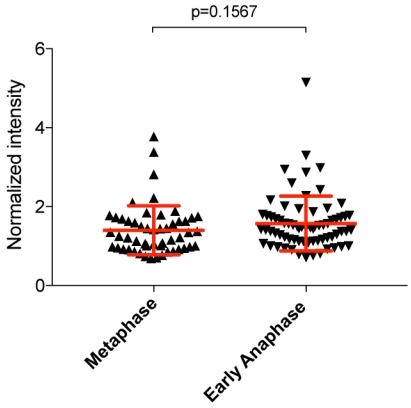

D Hela cytoplasmic actin (Live cells)

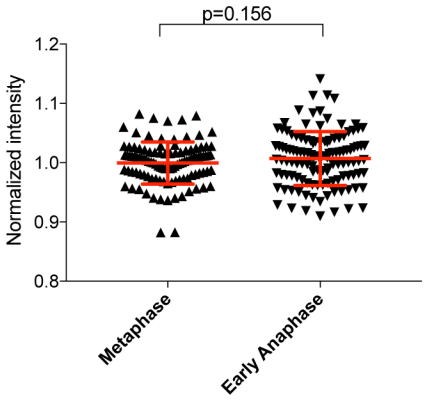

E

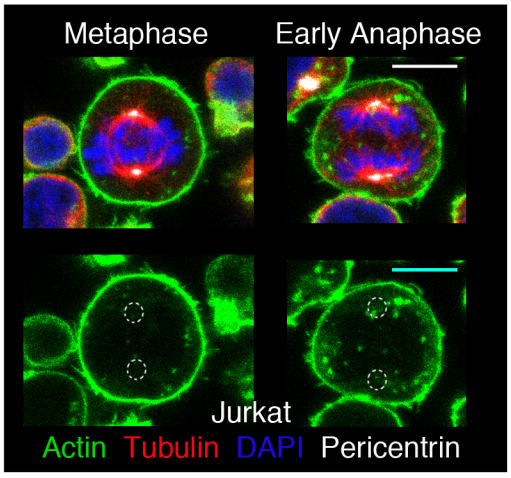

F

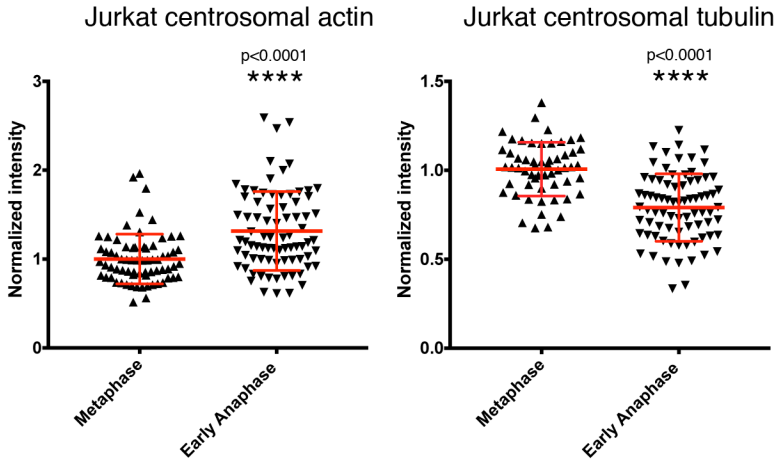

Supp Figure 2

A

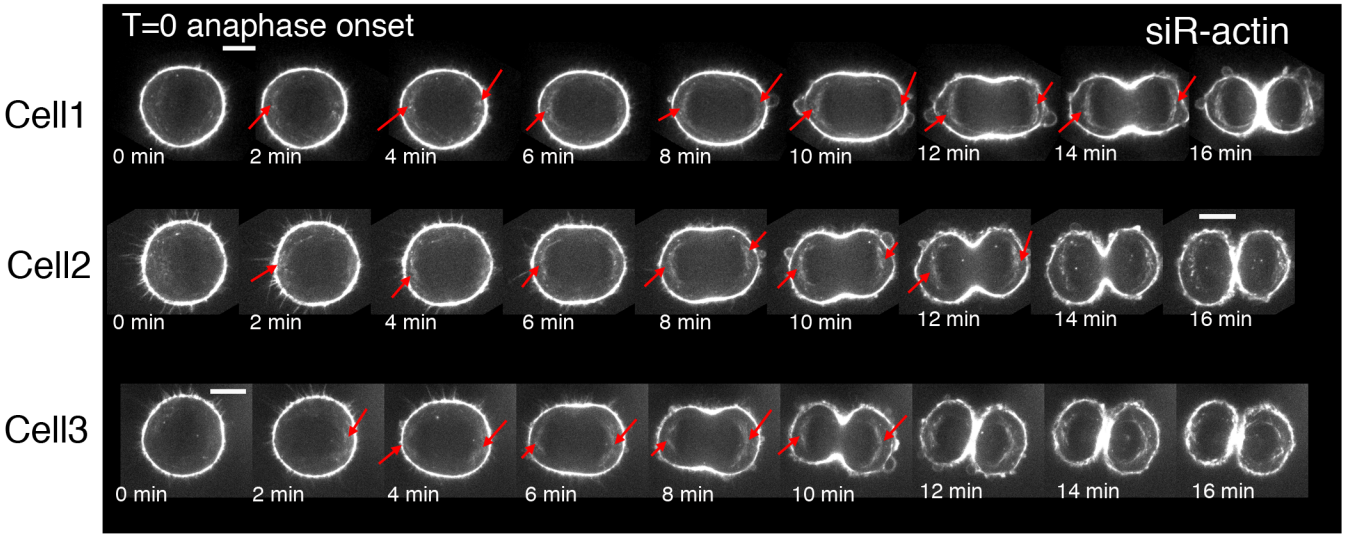

B

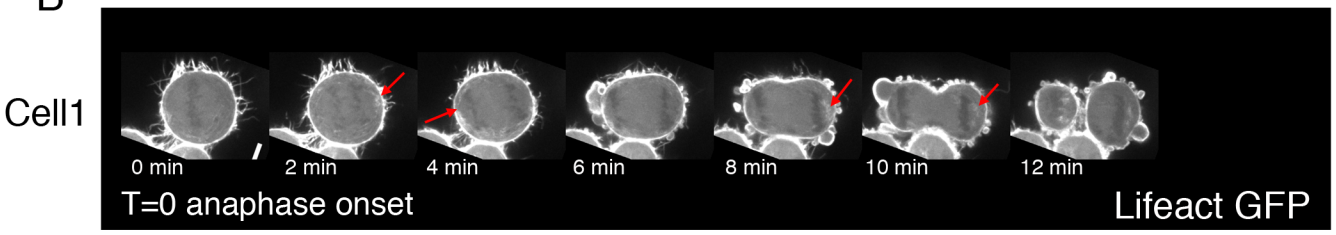

C

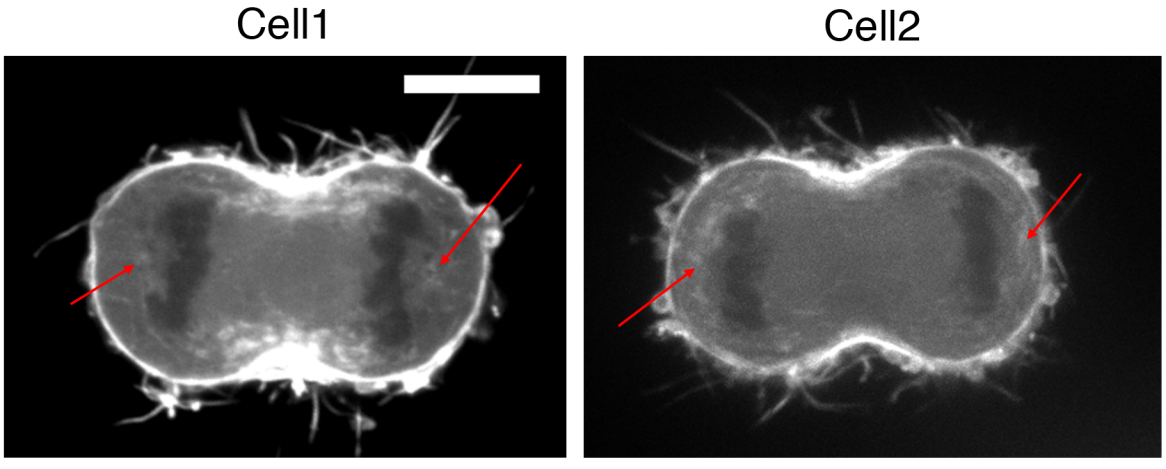

Supp Figure 3

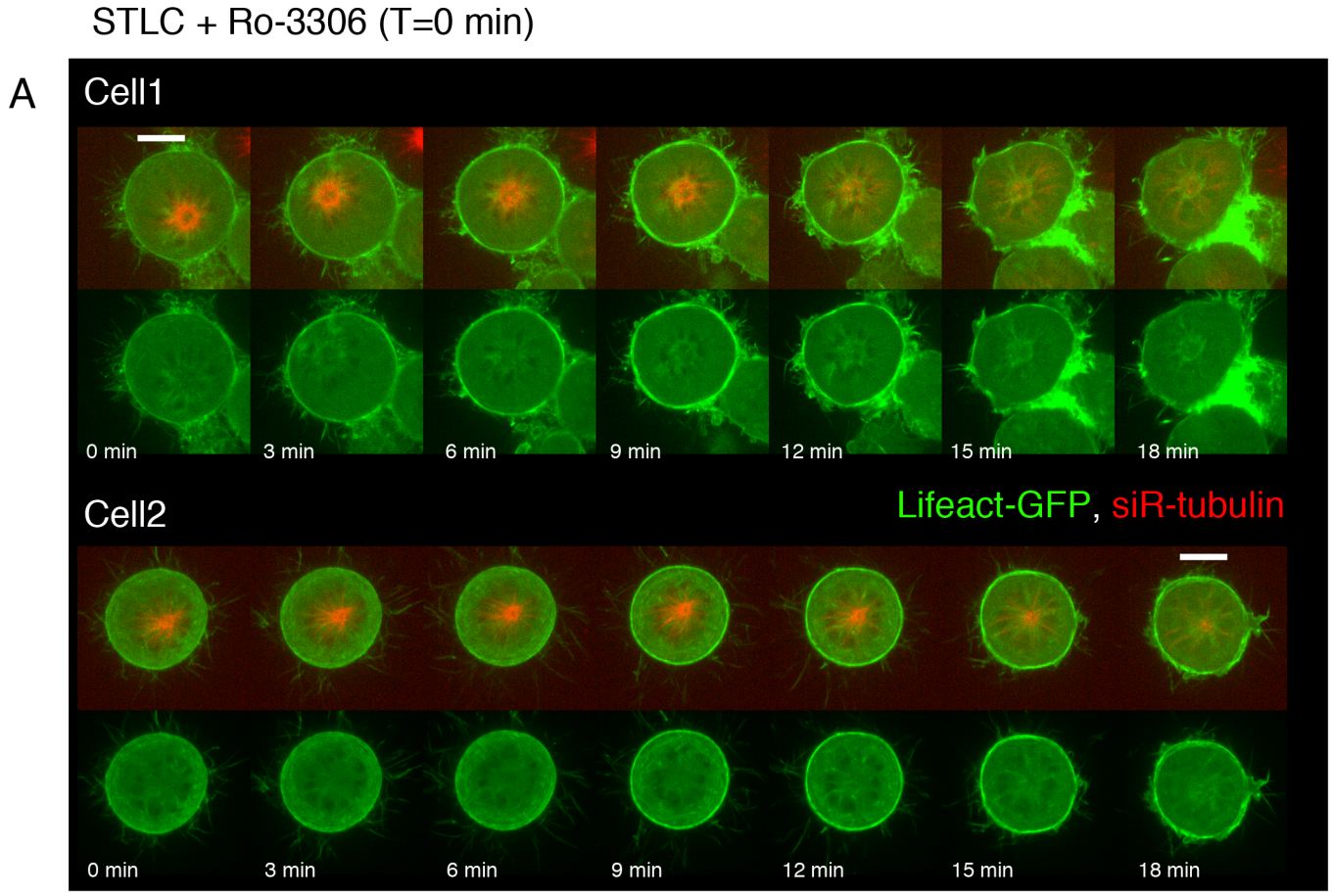

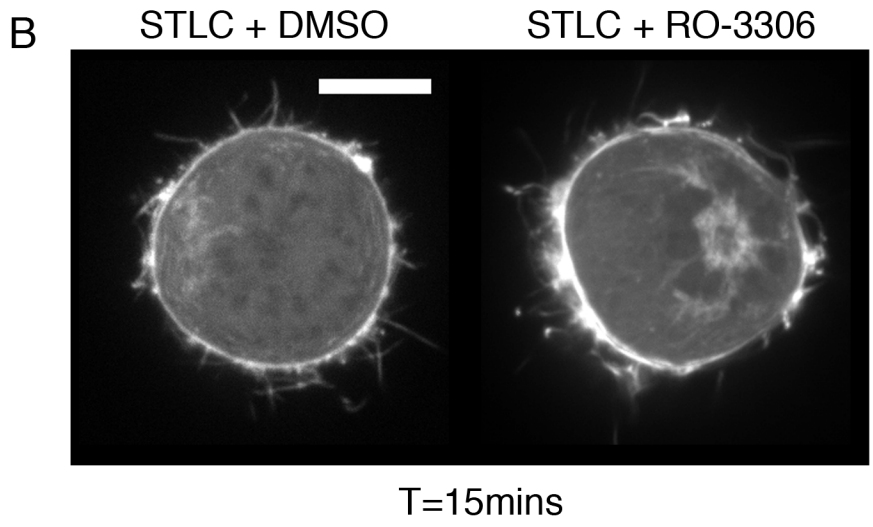

Supp Figure 4

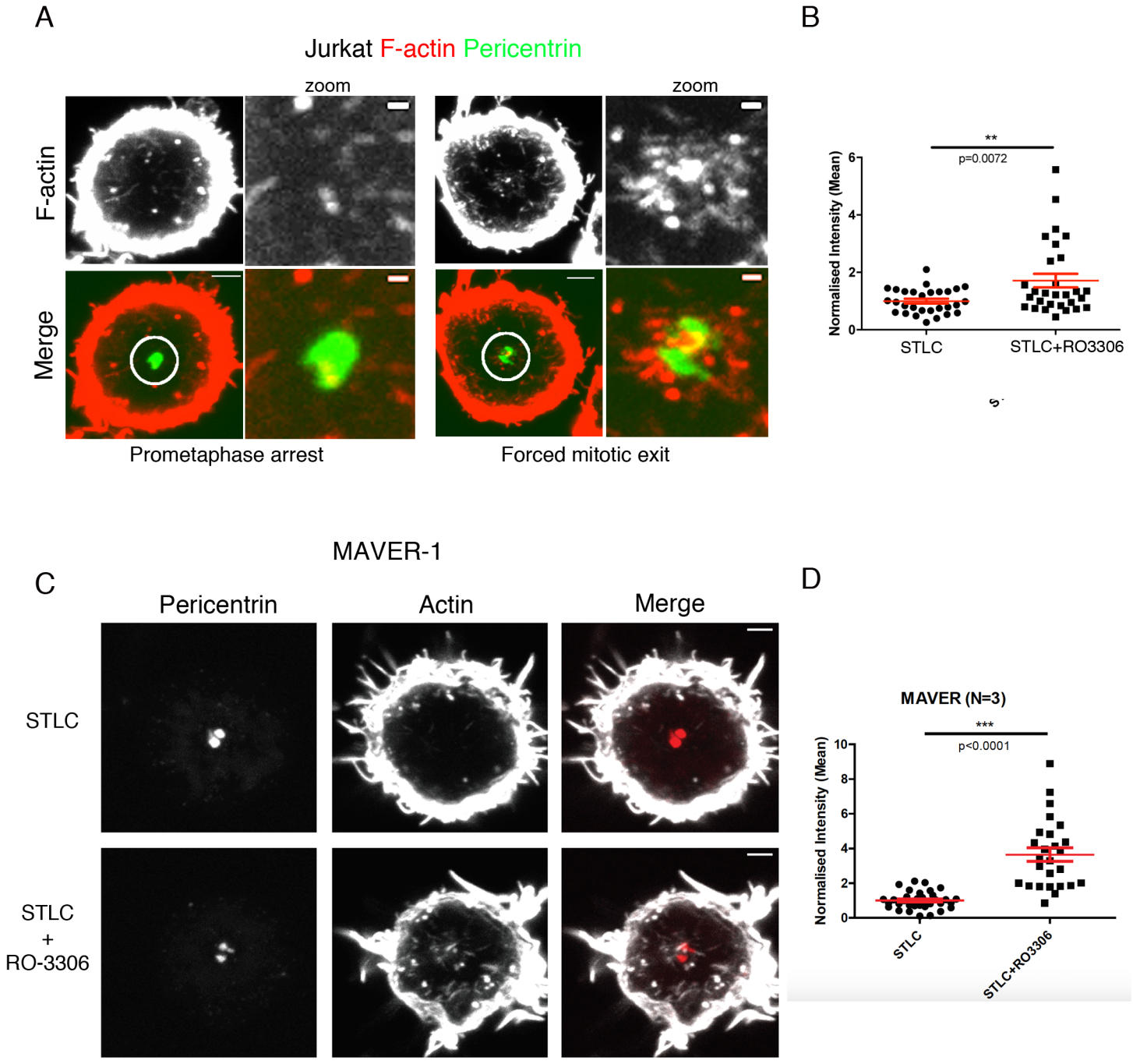

Supp Figure 5

A

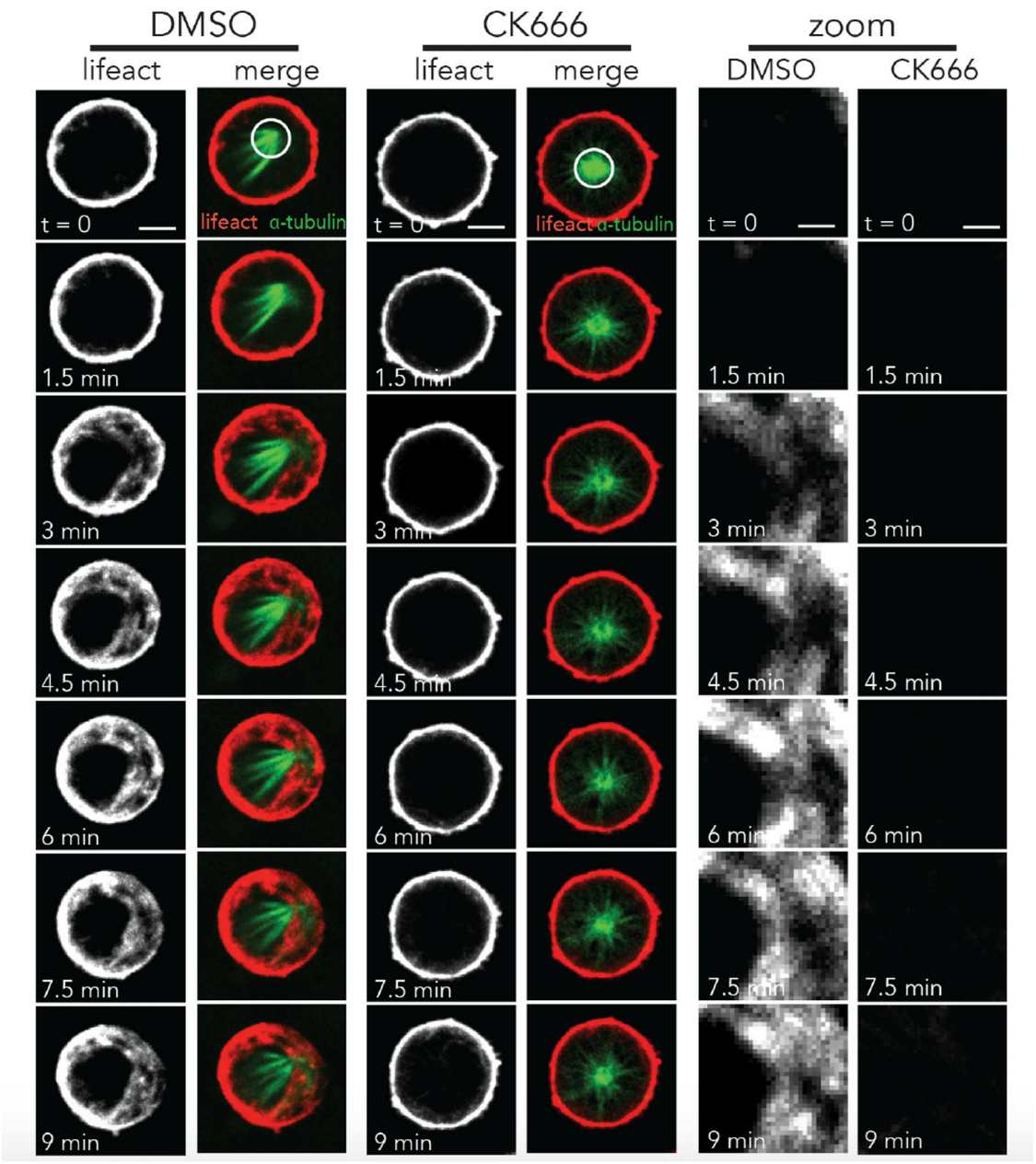

B

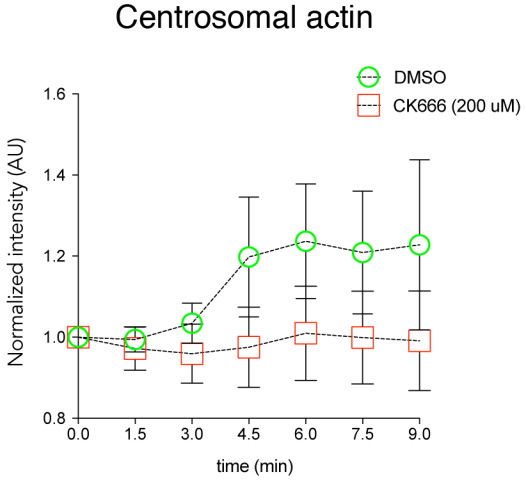

C

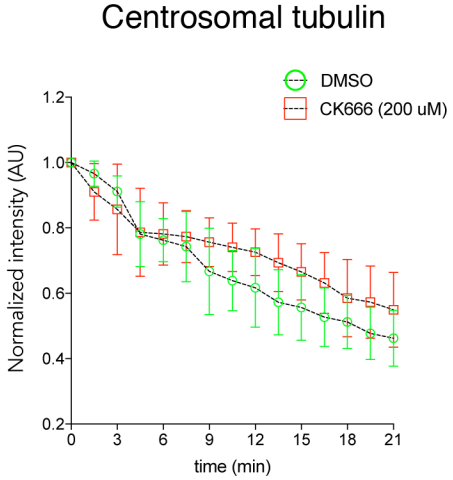

Supp Figure 6

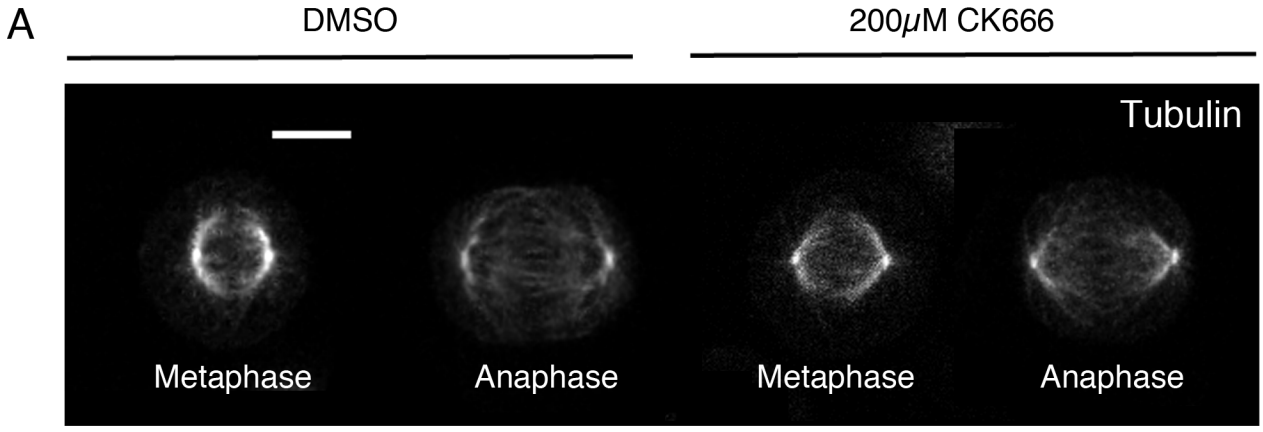

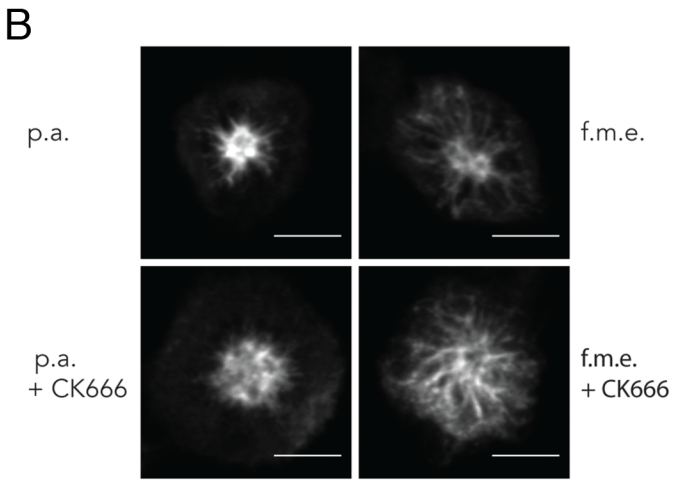

Supp Figure 7